SYNTHESIS AND FABRICATION OF HETERO-STRUCTURED METAL OXIDE NANOARRAYS AND THEIR CHARACTERIZATION FOR WATER SPLITTING APPLICATIONS

BY

AKRAM ABDALLA MOHAMMED IBRAHIM

A Thesis Presented to the

DEANSHIP OF GRADUATE STUDIES

KING FAHD UNIVERSITY OF PETROLEUM & MINERALS

DHAHRAN, SAUDI ARABIA

In Partial Fulfillment of the
Requirements for the Degree of

MASTER OF SCIENCE

In

CHEMISTRY

MAY 2016

KING FAHD UNIVERSITY OF PETROLEUM & MINERALS

DHAHRAN- 31261, SAUDI ARABIA

DEANSHIP OF GRADUATE STUDIES

This thesis, written by **Akram Abdalla Mohammed Ibrahim** under the direction of his thesis advisor and approved by his thesis committee, has been presented and accepted by the Dean of Graduate Studies, in partial fulfillment of the requirements for the degree of **MASTER OF SCIENCE IN CHEMISTRY.**

Dr. Ahsan Ul-haq Qurashi
(Advisor)

3/5/2016

Dr. Abdul-Aziz Al-Saadi

Department Chairman

Dr. Nisar Ullah
(Member)

Dr. Salam A. Zummo
Dean of Graduate Studies

Dr. Abdul-Rahman Al-Betar
(Member)

3/5/16

Date

Dedication

This thesis is dedicated to my parents, brothers and sister for their continuous prayer and support…

ACKNOWLEDGMENTS

I would like to thank my great creator almighty Allah for giving me life, health, strength patience, power and science to finish my study. Also, I would like to express my deepest appreciations to my thesis Advisor Dr. Ahsan Ul haq Qurashi for innovating and establishing research idea. And for his guides, encouragement, significant comments, and continuous help during the study.

I wish to extend my gratitude to my thesis committee Dr. Nisar Ullah and Dr. Abdul-Rahman Al-Betar for their valuable advice, encouragement and significant comments which supported me to complete this research.

It's my pleasure to acknowledge the Ministry of Higher Education (KSA), through the King Fahd University of Petroleum and Minerals for giving me this opportunity to presume my MS degree. My deep thank is extended to the Chemistry Department represented in our chairman Dr. Abdul-aziz Al-saadi and former Dr. Abd allah Al hamdan, also to Dr. Bassam El-Ali (Graduate coordinator) and to all faculty members and staff. My deep gratitude is extend to the center of excellence in nanotechnology where this research has been carried out, for their help and corporation. My thank is extended to Mr. Alaadin Abdella for his valuable support

It is my honor to thank all the institutions, centers, departments and people who guided and supported me to make this research endeavor a significant and successful.

TABLE OF CONTENTS

LIST OF TABLES

LIST OF FIGURES

LIST OF ABBREVIATIONS

PGSTAT	:	Potentiostat / Galvanostat
FESEM	:	Field emission scanning electron microscope
JCPDS	:	Joint Committee on Powder Diffraction Standard
$KJmol^{-1}$	:	Kilo Joule per Mole
LSVP	:	Linear Sweep Voltammetry Potentiostatic
DSSC	:	Dye Sensitized Solar Cell
IPCE	:	Incident Photon Conversion Efficiency
LEED	:	Low Energy Electron Diffraction
GLAD	:	Glancing Angle Deposition
EDS	:	Energy Dispersive x – ray Spectroscopy
ITO	:	Indium Oxide Tin Oxide Substrate
FTO	:	Fluorine doped Tin Oxide Substrate
AOPs	:	Advanced Oxidation Processes
STM	:	Scanning Tunneling Microscopy
STH	:	Solar To Hydrogen
DFT	:	Density Function Theory
PEG	:	Polyethylene Glycol
RSC	:	Royal Society of Chemistry
WWF	:	World Wide Fund
CVD	:	Chemical Vapor Deposition
PVD	:	Physical Vapor Deposition
SRM	:	Steam Reforming of Methane
OER	:	Oxygen Evolution Reaction

HER	:	Hydrogen Evolution Reaction
RHE	:	Reversible Hydrogen Electrode
NHE	:	Normal Hydrogen Electrode
HMT	:	Hexamethylenetetramine
CCD	:	Charge Coupled Detector
KSA	:	Kingdom of Saudi Arabia
NIR	:	Near Infrared
XRD	:	X – ray Diffractometer
PEC	:	Photoelectrochemical
Eqn	:	Equation
VIS	:	Visible
NRs	:	Nanorods
Min	:	Minute
Sec	:	Second
TO	:	Transverse Optical
LO	:	Longitudinal Optical
CA	:	Chronoamperometry
mA	:	Milliampere
UV	:	Ultraviolet
nm	:	Nanometer
eV	:	Electron Volt
Eg	:	Energy Gap
hv	:	Photon Energy
VB	:	Valence Band
CB	:	Conduction Band

MO	:	Metal Oxide
ΔG	:	Delta Free Energy
PL	:	Photoluminenscence
Pt	:	Platinum
AM	:	Air Mass
DI	:	Deionized
cm	:	Centimeter
Pa	:	Pascal
mm	:	Millimeter
mW	:	Milliwatts
DL	:	Deep Level
C	:	Celsius
M	:	Molarity
W	:	Watts
V	:	Volt
G	:	Global
R	:	Magnitude Reflectance
t	:	Time
H^+	:	Hydrogen Ion
e^-	:	Electron
h^+	:	Hole
β	:	Beta
Å	:	Angström
°	:	Degree
γ	:	Gama

λ	:	Lamda
θ	:	Theata

ABSTRACT

Full Name : Akram Abdalla Mohammed Ibrahim

Thesis Title : Synthesis and fabrication of hetero-structured metal oxide nanoarrays and their characterization for water splitting applications

Major Field : Chemistry

Date of Degree : May 2016

In this work we report hybrid synthesis of hetero-structured metal oxide nanoarrays namely ZnO/Ga_2O_3 and $WO_3/BiVO_4$ on desirable substrates for photoelectrochemical (PEC) water splitting under visible light. These hetero-nanostructured arrays were synthesized and fabricated by hybrid two-steps, physical approach and hydrothermal methods.

Hetero-structured ZnO/Ga_2O_3 was synthesized and fabricated on indium oxide tin oxide (ITO) substrate from alkaline (pH = ~13) aqueous solution containing ZnO and Ga_2O_3 individually. XRD analysis revealed that the fabrication of ZnO/Ga_2O_3 hetero-structured. FESEM characterization showed the formation of well-aligned nanorods arrays along with hexagonal shape on the entire surface of the ITO substrate. Optical properties confirmed the ability of ZnO/Ga_2O_3 thin film for harvesting visible light efficiently. Furthermore the photoelectrochemical properties was investigated under visible light with chronoamperometry (CA) and linear sweep voltammetry potentiostatic (LSVP) techniques. The photoresponse increased with increasing Ga_2O_3 amount and reached the peak value 0.60 mA/cm^2 with coating of thin layer of gold due to surface plasmon resonance of gold nanoparticles.

In addition $WO_3/BiVO_4$ hybrid metal oxide nanoflakes was synthesized and fabricated on (ITO) substrate from strong acidic (pH = ~1) aqueous solution containing WO_3 and $BiVO_4$ separately. XRD pattern showed the formation of $WO_3/BiVO_4$ hetero-structured metal oxide. FESEM analysis revealed the growth of nanoflakes. UV – VIS analysis explored the possibility of visible light harvesting of $WO_3/BiVO_4$ thin film. CA and LSVP were investigated for $WO_3/BiVO_4$ photoanode and illustrated the stability of thin film versus photo-corrosion and response enhanced with increasing annealing temperature. The peak value was 0.109 mA/cm^2 for $WO_3/BiVO_4$ thin film.

ملخص الرسالة

الاسم الكامل: أكرم عبد الله محمد إبراهيم

عنوان الرسالة: تحضير و تصنيع الأكاسيد المعدنية المختلطة و تشخيصها لغرض إستخدامها في تطبيقات تفكيك الماء.

التخصص: علوم الكيمياء

تاريخ الدرجة العلمية: مايو 2016

في هذا البحث تم تحضير وتصنيع بعض الأكاسيد المعدنية المختلطة مثل أكسيد الزنك/ أكسيد الجاليوم و أكسيد التنجستان/ أكسيد الفانديوم بزموث النانوية، علي بعض الأسطح (الموصلة) لإستخدامها في تفاعلات تفكيك الماء عن طريق التفاعلات الكهروضوئية باستخدام الضوء المرئي. هذه الأكاسيد المعدنية المختلطة تم تحضيرها في خطوتين بطريقتين مختلفتين الطرق الفيزيائية و الطرق الحرارومائية.

التركيبة المختلطة من أكسيد الزنك/أكسيد الجاليوم تم تحضيره و تثبيته علي سطح زجاجي موصل مصنوعة من أكسيد الإنديوم و أكسيد القصدير في محلول مائي قلوي (الرقم الهيدروجيني = 13~) تحتوي علي أكسيد الزنك و أكسيد الجاليوم . تحليل أشعة الحيود السيني أشار الي تكون التركيبة المختلطة من أكسيد الزنك/أكسيد الجاليوم. التشخيص بواسطة المسح السطحي عن طريق المجهر الإليكتروني أشار الي تكون أعواد نانوية قائمة مع الشكل السداسي علي سطحه فوق كل السطح الزجاجي (الموصل). الخواص الضوئية لهذا التركيبة المختلطة من أكسيد الزنك/أكسيد الجاليوم تم دراسته بواسطة جهاز مقياس الأشعة فوق البنفسجية و أشار الي أن هذا الخليط يستطيع أن يمتص الضوء المرئي بكفاءة عالية. بالإضافة الي أنه تم دراسة مقدرة الأكسيد المختلط علي الإستجابة للضوء بإستخدام الضوء المرئي بتقنية الكرونوأمبيروميتري و لينير إسويب فولتاميتري . هذه الإستجابة للضوء المرئي تطور مع زيادة تركيز أكسيد الجاليوم و وصل أعلاها (0.60 ملي أمبير/سم^2) مع إضافة عنصر الذهب و عزي هذا الي الرنين البلازموني السطحي لجسيمات الذهب.

أما التركيبة المختلطة من أكسيد التنجستان/أكسيد الفانديوم بزموث تم تحضيره و تثبيته علي السطح الزجاجي (الموصل) المصنوع من خليط أكسيد الإنديوم و أكسيد القصدير من محلول مائي عالي الحمضية (الرقم الهيدروجيني = ~1) يحتوي علي أكسيد التنجستان و أكسيد الفانديوم بزموث. تم التأكد علي تكون التركيبة المختلطة

أكسيد التنجستان/أكسيد الفانديوم بزموث بواسطة أشعة الحيود السينية. التشخيص بواسطة المسح السطحي عن طريق المجهر الإليكتروني أشار الي تكون رقائق نانوية. تم التأكد أيضا علي مقدرة التركيبة المختلطة من أكسيد التنجستان/أكسيد الفانديوم بزموث علي إمتصاصه للضوء المرئي بواسطة جهاز مقياس الأشعة فوق البنفسجية. و عليه تم دراسة تقنية الكرونوأمبيروميتري و الينير إسويب فولتاميتري للتركيبة المختلطة أعلاه وتبين أن هذا الأنود ثابتة ضد التآكل الضوئي، و أن الإستجابة للضوء المرئي تضاعف مع زيادة درجة حرارة التصليب وسجل أعلي إستجابة عند (0.109 ملي أمبير/سم^2).

CHAPTER 1

INRODUCTION

1.1 The energy crisis:

As a result of revolution of the industry the demand of energy has been increased as well as due to an exponential increase of the world population. At the moment there are over seven billion in the globe, utilizing 15 TW of energy. By 2050, it is expected that ~ 9 billion will be in the world and 30 TW is required from energy. The major challenge to the world nations is to providing enough amount of energy. Currently over 80 % of the required energy are producing from fossil fuels, i.e. natural gas, oil and coal see Figure (1). However, these are limited resources of energy, and their depletion rate is too high. Although, there are information expecting that the current energy resources reserves are sufficient for centuries, the reserves diminishing will be touched soon, due to many of these reserves are inappropriate, which is reflected by the challenges of the extraction procedures. Thus, the supply demand associated is no longer flexible. Since 2005 the international production of oil reached 75 million barrels daily, there are fluctuating in international price of oil between 40 to 130 US$ per barrel [1]. For extra elaboration of this urgent issue, the WWF lately announced a report indicating that if anyone in the globe utilized oil at the similar rate of US resident, Saudi, or Singaporean the international reserves of oil should be diminished in less than 10 years [2]. The major cause of the climate change is carbon dioxide (CO_2), which is producing from emission of greenhouse gas as a result of relying on fossil fuels. The reported data show that more

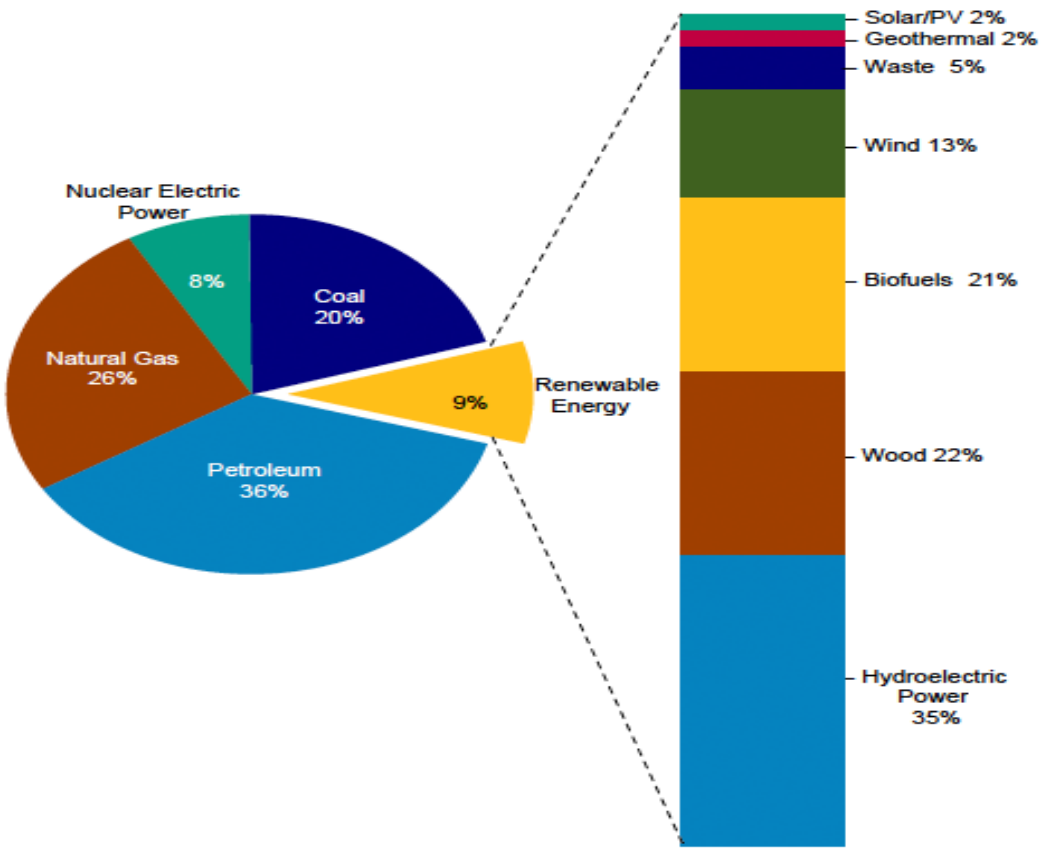

Figure 1: Renewable energy as share of total primary energy consumption, 2011. U.S energy information.

than 150,000 deaths annually [2] due to climate change, this encouraged to search alternative, clean, emission free source of energy instead of fossil fuel. With the starting of the industrial revolution the CO_2 level in atmosphere was 280 ppm, this level has been increased significantly up to 400 ppm recently [3] with increasing rate of ~2 ppm/year.

The international panel on climate change (IPCC) proposed for keeping the CO_2 level below 450 ppm to avoid increasing in the global temperature more than 2 °C [4]. To get opportunity of pursuing that with next 5 years, the emission of greenhouse gas necessity required to decline along with reduction of industrialized world up to 20 % as

in 1990 [5]. The work above is very huge, however it is fortunately possible utopia. Ecofys mentioned methods to overcome this problem experimentally with possible solutions [5]. These methods it can be seen in Figure (2). The below methods might encourage, potential solution. Government, scientist and industries etc. need to work as a team and they need to begin as soon as possible. The optimal transition route from the current fuels to renewable source is a big argument. Technological consideration and its economic advantage need to be investigate. First of all renewable and sustainable energy sources have to be used as alternative of fossil fuels in a large scale, to decrease the emission of the greenhouse gases by around 80 % from energy sector within 30 coming years. As a second option electrification policy and crucial condition need to adjust for energy saving. Thus, it is expected that the required energy by 2050 will be around 15 % less than in 2005.

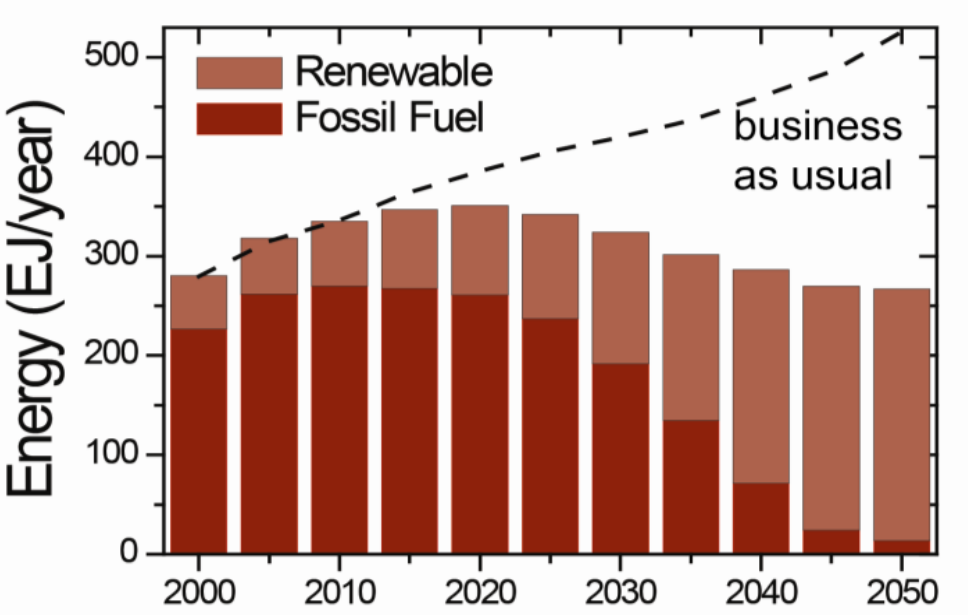

Figure 2: Ecofys scenario for fossil fuel to renewable energy transition.

1.2 Motivation and Background:

Clean energy is one of the major problem of 21th century. Global population has passed seven billion. Technology are expected to supply [~ 20 – 40 terawatts] of energy for human around the world. Although this significant increase in demand non-renewable source is the main source of fuels. Thus this led to contamination, climate changed and reduced the quality of human and planet life globally. To overcome this problem without affecting our planet, producing energy from renewable energy sources was proposed as alternative fuels such as wind, biomass and water etc. After the effort of Fujishima [6] to produce hydrogen from water using Titania hydrogen was proposed as future fuels. Hydrogen is promising candidates as future fuels, because it is free emission and clean energy source. Photocatalytic and photoeletrochemical water splitting have received a great deal of attention because it can overcome the pollutions [7] by direct conversion of solar power into chemical energy such as hydrogen. In contrast the efficiency of conversion of solar to hydrogen by Titania is basically restricted due to large band gap 3.2 eV that limited the response to UV region and recombination of carrier charge was very high [8]. Different methods were utilizing to produce hydrogen from various source such as steam reforming of methane gas (SRM) in two steps process, reaction of methane gas with water vapor in the presence of catalysis and elevator temperature following by reaction of carbon monoxide with water vapor at low temperature, secondly production of hydrogen from cool (gasification) and drawbacks of both methods are the emissions of CO_2 and non-renewable sources. Another method to generate hydrogen is water electrolysis and this may utilize high energy and an expensive. The most attractive and promising one is the production of hydrogen using solar energy. Although water splitting is an expensive but it is the most favorable and

promising method because it is highly efficient and free emission energy source. A number of semiconductors such as TiO_2 and $SrTiO_3$ have been demonstrated to have the ability to split water under ultraviolet (UV) light irradiation. However, less than 5% of the total solar energy that illuminates earth is in the form of UV. Thus numerous effort have been made to improve the photocatalytic materials that can utilize the visible region of the solar spectrum such as cation doping, anion doping and formation of hetero-structure metal oxide. Formation of hybrid metal oxide is the most promising aspect such as $WO_3/BiVO_4$ and ZnO/Ga_2O_3 because it is inexpensive, chemically and mechanically stable and have desired band gap.

In the recent years, there is an increasing demand of nanomaterials. Nanomaterials are in the form of nanoparticles, nanowires, nanotubes and nanorods etc. The rising demand is because of their properties. It is believed that hetero-structured metal oxides nanoarrays have large site of interaction, so it can allow the improvement of properties with completely modified electronic structure and the band gap absorb visible light. $BiVO_4/Co_3O_4$, and WO_3/Fe_2O_3 are examples of nanostructured films of hetero-junction which can improve the charge separation. Mixture of metal oxides nanotubes / nanosheets which can provide high surface area and narrower band gap, are good candidate to produce hydrogen through photoelectrochemical process. In this context, hetero-structure metal oxide nanoarrays, such as Cu_2O/TiO_2, $WO_3/BiVO_4$, and ZnO/Ga_2O_3 have emerged as the most promising candidates as photocatalysts for hydrogen production from water due to their high chemical stability, synthetic feasibility and desired band gap [9, 10, 11]. However the selection of the materials for practical PEC water splitting is limited. Figure (3) represent the band edge and band gap place of

representative semiconductors. They should be stable in strong alkaline and /or acidic conditions for excellent electrolyte conductance. Band gaps should be higher to recompense unavoidable voltage losses, for instance electrode over-potentials and device series (ohmic) resistance.

Among metal oxides, only large band gap ones such as TiO_2 and ZnO can cover the water reduction and water oxidation potentials [12]. However, the large band gap (only responsive to UV light (<400 nm) limits their visible light absorption and photoelectrochemical water splitting. On the other hand, small band gap metal oxides such as WO_3 possess conduction band potentials more positive than water reduction potential, and hence, the application of external voltage are necessary to split water. Therefore, development of visible-light driven photocatalysts that can efficiently convert the solar energy into chemical energy and inhibit the electron-hole recombination is highly demanding. Many approaches were developed in terms of preparation of hetero-structured metal oxides in nanoscale level such as chemical vapor deposition (CVD), sol – gel and hydrothermal methods etc. Among these, our targeted materials will be prepared by hybrid physical appraoches and hydrothermal method to grow metal oxide on the suitable substrate such as fluorine doped tin oxide (FTO) glass coated substrate or indium oxide tin oxide (ITO) substrate. Photoelectrochemical (PEC) water splitting is a process that use an external source of electricity to split water. In recent years [13] advanced oxidation processes (AOPs) have been suggested as various approach for the degradation of recalcitrant organic compounds in air [14], soil [15] and water [16]. Heterogeneous photoelectrochemical received great attention among the AOPs [17]. This approach mainly rely on the illumination of the semiconductor with solar energy greater

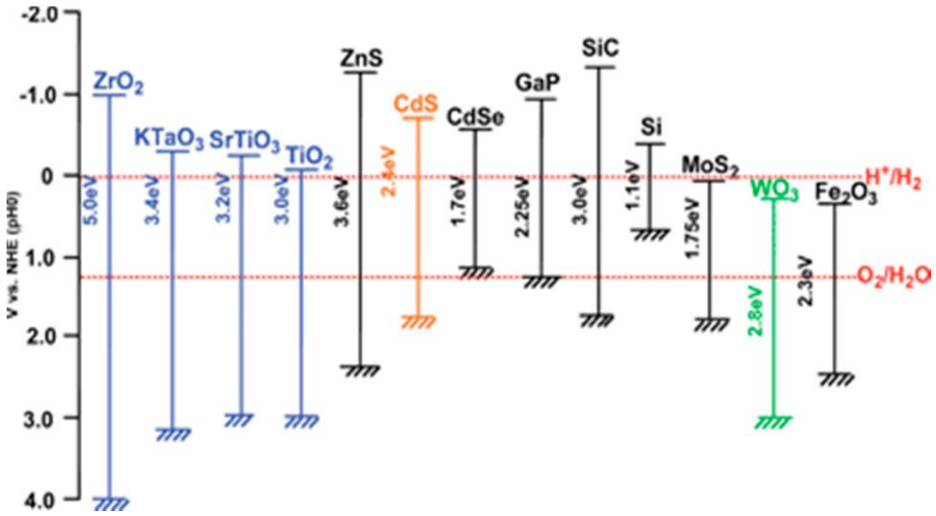

Figure 3: Band gaps and edges positions of representative semiconductors in relation to the redox potential for water splitting at pH =0 [Reproduced with permission of the RSC]

or equal to the semiconductor band gap energy. Semiconductors are materials identified by two bands of energy isolated by the band gap energy, Eg. At absolute zero semiconductor is insulating, due to occupation of valence band and unoccupation of conduction band. Charge carrier need to be formed in order to make it conductive, as usual via photoexcitation. The fundamental principle is that when the surface of thin film semicondutor is illuminated by light ($h\nu \geq Eg$) energy, there is formation of an electron/hole pair (e^-/h^+) by the transfer of electron from valence band (VB) to conduction band (CB) equations **1 – 4** [17,18].

$$MO + h\nu \longrightarrow MO\text{-}e^-_{CB} + MO - h^+_{VB} \qquad \text{Eqn (1)}$$

$$H_2O + h^+ \longrightarrow \tfrac{1}{2}\, O_2 + H^+ \quad \text{(OER; Oxidation)} \qquad \text{Eqn (2)}$$

$$H^+ + 2e^- \longrightarrow H_2 \text{ (HER; Reduction)} \qquad \text{Eqn (3)}$$

$$H_2O \longrightarrow \frac{1}{2} O_2 + H_2 \ (\Delta G = +237.2 \text{ KJ mol}^{-1}) \qquad \text{Eqn (4)}$$

Despite heterogeneous photoelectrochemical is promising and applying in water splitting, however its experimental utilization has been limited due to its low photonic efficiency, due to recombination of the e^-/h^+ pair as mentioned in the equation **5** [19,20].

$$MO - e^-_{CB} + MO - h^+_{VB} \longrightarrow MO + \text{heat} \qquad \text{Eqn (5)}$$

Many attempt have been carried out to isolate charge carriers and decrease their recombination rate [20, 21]. The incorporation of photocatalysis and electrochemical process offer opportunity to isolate photo-generated e^-/h^+ pairs by gradient potential [22,23]. Particularly, when the photocatalyst is in contact with the conductive substrate (photoanode), there is the chance to apply an anodic bias potential to the semiconductor and to modify the substrate /electrolyte interface. This process enhance the charge isolation efficiency by driving the photo-generated electrons by external circuit to the counter electrode [20, 22-24] the mechanism of photoelectrochemical water splitting showing in Figure (4). The significant part of photoelectrochemical water splitting is the catalytic materials used as photoanode in the water splitting process. Water splitting requires effective electro-catalysts to produce hydrogen to attain high current density at low over-potential. The efficiency is enhanced when platinum (pt) used as the catalysts. However, pt remains as an expensive metal and suffers from a shortage in global supply [25, 26] alternative materials have been considered. Low cost, earth abundant tungsten, bismuth, vanadium, gallium and zinc electro-catalysts are considered as the most promising alternatives catalysis for efficient hydrogen generation instead of pt, which attracted numerous researchers' interests. Among those electro-catalyst, hetero-structured

metal oxide nanoarrays have been reported to exhibit catalytic activities for the water splitting [27, 28]. However, solar energy offers a clean, abundant and unlimited energy resource to man-kind and provides a green way to fulfill the global demand for free emission energy [29]. The sunlight provides us with a wide range of spectrum of applications such as solar heating, photovoltaics, photoelectrochemical water splitting, photosynthesis, and photocatalysis. Hydrogen generation through photoelectrochemical (PEC) water splitting using solar light as an energy resource is believed to be a clean and efficient way to address the global energy and environmental problems [30,31,32]. The solar radiation in Kingdom is very intense and development of active materials that can harvest the solar energy will significantly contribute to the economy of the Kingdom of Saudi Arabia.

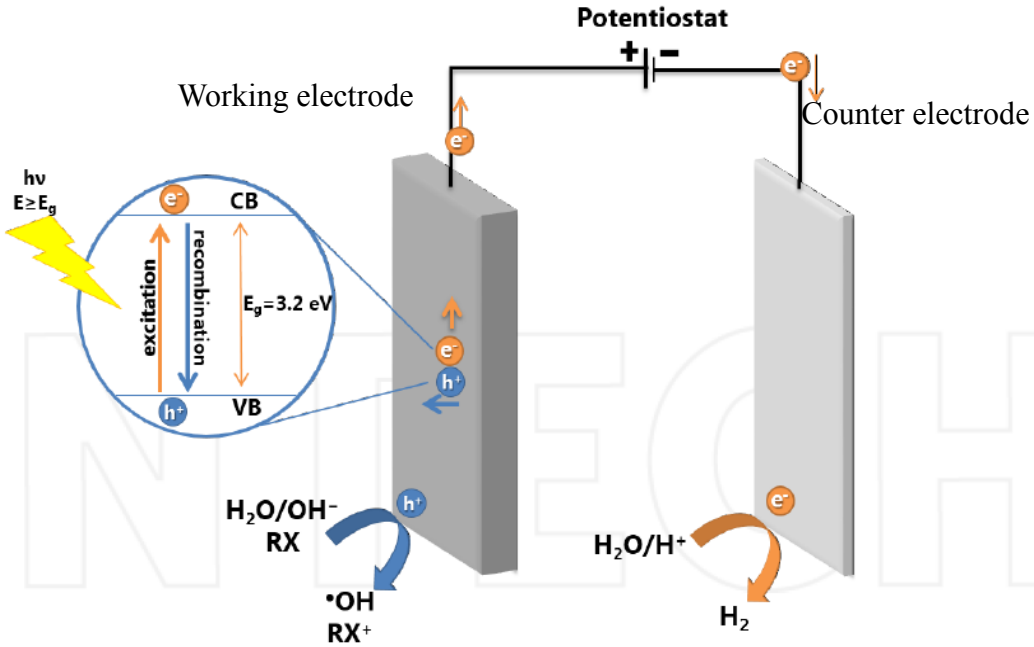

Figure 4: Schematic illustration of charge separation and recombination mechanism in the photoelectrochemical process where gradient potential is created

1.3 Aim of the Study:

Pollution is the serious problem against environment, because it has negative impact on the land, water and air we breathe. For instance airborne nitrogen pollution, carbon dioxide emissions (CO_2) and acid rain. These problems raises due to human activities from depending on fossil fuels. When fossil fuels burned by humans they emit carbon dioxide (CO_2), nitrogen oxide (NO_X) and Sulfur oxide (SO_X) into atmosphere. As a result of releasing these materials into atmosphere climate changed, acid rain etc. to overcome this problems many steps have been considered, one of them is to replace fossil fuels by renewable energy sources such as water, biomass and winds etc. since hydrogen proposed as alternative fuels, our aim in this study is to split water into hydrogen and oxygen through environmental benign methods. Furthermore we aim to develop materials that can harvest visible light to perform water splitting. These materials should have desired band gap and free from defects.

1.4 Methodology:

Preparations of thin films were performed using two steps hybrid method for both ZnO/Ga_2O_3 and $WO_3/BiVO_4$ thin film which are physical approach using sputtering and wet chemistry (hydrothermal approach) according to literature [33,34], by mixing the precursor solutions for each metal. These synthesized nanoarrays and naoflakes metal oxides were characterized by X – ray diffractometer (XRD), field emission scanning electron microscope (FESEM), energy dispersive X – ray Spectroscopy (EDS), and Raman Spectroscopy. The optical properties of those materials were studied by

photoluminescence (PL) and UV – VIS Spectroscopy. photoelectrochemical cell was developed for water reduction and oxidation. Metrohm autolab (B.V) potentiostat/galvanostat PGSTAT 10 used as a potential source, visible light was created using solar simulator (oriel) class 3A along with 1.5 AM (1sun).

1.5 Research Objectives:

1. To synthesis and fabricate binary semiconductor zinc oxide/gallium oxide hetero-juction (ZnO/Ga_2O_3) photoanode nanoarrays.
2. To synthesis and fabricate tertiary semiconductor tungsten oxide/bismuth vanadium oxide ($WO_3/BiVO_4$) hetero-junction photoanode nanoflakes.
3. To characterize them using standard methods such as XRD, FESEM, UV - VIS and Raman spectroscopy.
4. To develop photoelectrochemical cell for water splitting under visible light.

1.6 Thesis Organization:

As for the structure of this thesis, it is divided into five (5) main chapters. It starts with the introduction and motivations **in Chapter one (1)**, where the aim of the study, main objectives, the methodology and technique are presented. This is followed by a brief review of related literature **in Chapter two (2)** about the crystal and nanostructure of ZnO, Ga_2O_3, WO_3 and $BiVO_4$. In addition to configuration of hetero-structure of ZnO/Ga_2O_3 and $WO_3/BiVO_4$ photoanodes for water splitting. **In chapter three (3)** the synthesis and fabrication of ZnO/Ga_2O_3 thin film are showed with broad details. This include all steps of experimental from synthesis and characterizations with different

technique, furthermore results and the discussions of the formation of ZnO/Ga_2O_3 hetero-structure followed by the photoresponse and linear sweep voltammetry potentiostatic as an indication of water splitting. Synthesis and fabrication of $WO_3/BiVO_4$ photoanode are discussed with more details **in chapter four (4).** All practical's methods with identifications tools in addition to scientific interpretations of the photo-activity of the $WO_3/BiVO_4$ photoanode. The outcome and conclusion of this study with brief recommendation have been presented **in chapter (5).**

CHAPTER 2

LITERTURE REVIEW

2.1 Zinc Oxide/Gallium Oxide Nanoarrays for Water Splitting:

2.1.1 Zinc Oxide Nanostructure:

Semiconductor metal oxide nanoarrays with high surface area and small diffusion length are classified as photoanode/electrode materials that can split water under solar light via photoelectrochemical process. Nb_2O_5, CeO_2, ZrO_2, ZnO are examples of different metal oxides have been tested as photoanodes in solar cell. In contrast the benefit given by high surface area of nanostructure is restricted due to charge collection by the photoelectrode. Well – aligned nanoarrays with high crystallinity was improved and developed for rapid charge transfer in solar cell. Grätzel et al reported that high surface area of TiO_2 nanocrystal has been covered by a monolayer of dye molecule to harvest solar light. Zinc (II) oxide demonstrated larger electron transfer for the typical conduction band energies and band gap in comparison with titania.

Dye sensitized solar cell (DSSC) is favorable candidate as alternative energy devices because it is inexpensive and highly effective. Certain attempts have been concentrated in applying zinc oxide in dye - sensitized DSSC. Baxter et al applied zinc oxide nanowire in DSSC as photoelectrode, The outcomes of baxter configuration of solar cell was 1.3 mA/cm^2 in terms of photocurrent , 0.7 V, 0.3% and 0.35 – 0.40 as photovoltage, total efficiencies and fill factor respectively. Electron transfer via the nanoarrays is not enforced by nanoarrays dimensions. Wang et al used facile and inexpensive approach for

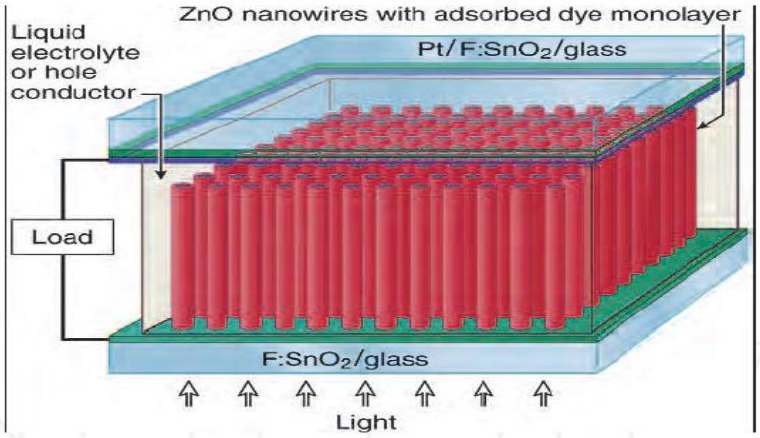

Figure 5: Schematic illustration of nanowire-based dye-sensitized solar cell.

preparing ZnSe/ZnO core-shell nanoarrays on large area, transparent, conducting substrate. Optical and structural properties have been investigated by different technique. Photoconductivity and absorption measurement gave an enhanced photoresponse for ZnO band gap. Figure (5) illustrate crystal structure of ZnO nanostructured in relation to the photoelectrochemical properties.

2.1.2 Crystal Structure of Zinc Oxide:

Wurtzite ZnO has crystal structure with hexagonal phase (space group C_6mc), lattice data c = 0.52065 nm and a = 0.3296 nm. ZnO structure briefly can be explained as a construction of different planes coordinated tetrahedrally in Zn^{2+} and O^{2-} ions see figure (6). Arranged alternatively with c-axis. Pyroelectrically and piezoelectrically obtained as a result of non-central symmetric of tetrahedral coordination of zinc oxide. Polar surface is other vital properties of zinc oxide. Basal plane is well known polar surface of ZnO. Variation of surface energy in addition to spontaneous polarization and normal dipole moment in ZnO obtained as arrangement of positive Zn – (0001) and negative charged O

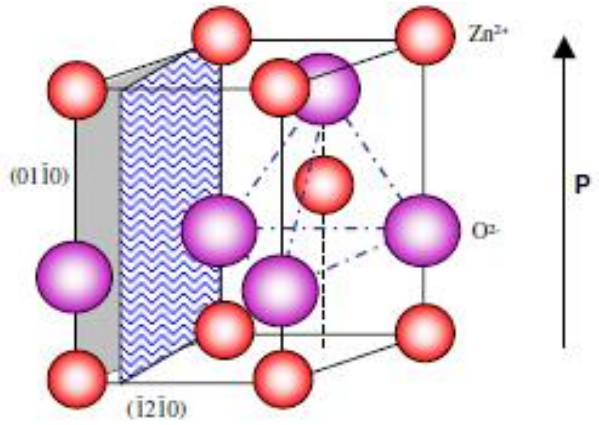

Figure 6: Wurtzite structure of ZnO the tetrahedral coordination of Zn - O is given

– (000-1). Nemours effort of reconstruction of surface have been paid to the polar surface of ZnO in order to get stabilized structure. Zinc oxide with plane phase ±(0001) are stable and flat even in the absence of intensive construction [35, 36]. [2-1-10] and [01-10] various facets of ZnO which are non-polar surface and have less energy than [0001] facets. Much work have been carried out to understand the high stability of zinc oxide ± (0001) polar surface nowadays in physics surface research [37- 40].

2.1.3 Gallium Oxide Nanostructure:

Much attention have been given to study gallium ability in hydrogen production from water under solar energy, after the effort of inoue et al by $ZnGa_2O_4$ zinc gallate [41]. They noticed overall water dissociation at maximum rate of 40 $\mu molh^{-1}g^{-1}$ by using RuO with zinc gallate. Domen et al [42] reported enhancement in hydrogen production rate to 3300 $\mu molh^{-1}g^{-1}$ in a solid solution of zinc oxide and gallium nitride formed from dissociation of zinc gallate. Zinc (II) oxide and gallium (III) oxide nitridation produce $(Ga_1 – xZn_x)$ $(N_1 – xO_x)$, which possess higher quantum efficiency and excellent stability.

Production of hydrogen was enhanced than previously mentioned which is ~200 μmol $h^{-1}g^{-1}$ when the co – catalyst replaced by transition metal in existence of chromium [43]. In particular Rh, Pt, Ni and Cu when these metal loaded as co – catalyst in the presence of Cr, hydrogen production rate raised 13000, 2600, 2300 and 1950 μmol $h^{-1}g^{-1}$ respectively [44]. At 300 – 340 nm the catalysis performance enhanced by 4 % as well as at 420 – 440 nm to 2.5 % when the mixture oxide of ruthenium: chromium used as co – catalyst [45].

In one study gallium nitride was synthesized by two different preparation approaches from nitridation of gallium oxide and elemental gallium. Even the loaded co – catalyst were activated in two approaches for complete water dissociation, hydrogen was generated in higher rate for elemental gallium approach comparing to the Ga nitridation approach, and the highest rate obtained was 63 μmol$h^{-1}g^{-1}$ [46]. By raising nitrogen doped amount up to 3.5% in GaPN the activity can enhance by ~8 and current density of 12 mA/cm^2 at 1V [47]. This idea published by turner and his co – workers in different gallium dependent catalyst. By adding arsenic to the lattice GaAsPN produced which possess 1.73 – 1.88 eV as a range of band gap. Although GaAsPN has extremely small band gap, the achievement of GaAsPN was little because minor carrier transfer in addition to flat band potential it is more negative for water dissociation [47]. $GaInP_2$ was somehow different, Even in low band gap energy of 1.83 eV the structure produce photocurrent around 28 – 30 mA/cm^2 at an illumination ~5 solar energy [48], because the gallium dissolution photocurrent decreases with time. Rapid charge transfer and low recombination rate can be improved by direct proportion between light intensity and photocurrent.

2.1.4 Crystal Structure of Gallium Oxide:

Gallium oxide and gallium hydroxide are excellent candidate materials for large widow of device applications. β-Ga_2O_3 has a monoclinic crystal structure with dimensions a = 12.23, b = 3.04, c = 5.80 Å and β = 103.7° [49, 50]. Four gallium oxide exist in the unit cell. The most possible space group is the crystal belong to C_{2h}^3-*C2/m*, that is atoms are in the 5 sets of particular places 4i: (000, ½ ½ 0) ± *(*x0z). Ga^{3+} ions has two type of coordination in that structure, exactly octahedral and tetrahedral. Inter-ionic distance in average are: octahedron edge O-O (2.84 Å), tetrahedral edge O-O (3.02 Å) octahedral Ga-O (2.00 Å) and Ga-O tetrahedral (1.83 Å). α-Ga_2O_3 has α-corundum structure as in Figure (7), where oxygen ions are located relatively in hexagonal closed – packed array with whole Ga^{3+} ions coordinated octahedrally to O^{2-} ions, and density is higher than β-Ga_2O_3 because of decreased coordination of half metal ions, the metal ions become very close to each other also in the α-phase because the octahedral share faces and edges. The shortest distance between Ga^{3+} - Ga^{3+} polyhedra is 3.04 Å in addition with no face sharing [50].

In general the structure which edges of polyhedral are shared is most stable than those of face are shared, which implying that are less stable than the only corner shared structure [51]. Therefore one could predict the α-phase to be less stable than β-phase. Foster et al. reported that despite the α-Ga_2O_3 produced by less temperature than β-Ga_2O_3, the α-phase is metastable [52]. Beta gallium oxide it is most stable gallium oxide phase with promising optical and electrical character at high temperature. Because the vacancies in oxygen in the crystal β-Ga_2O_3 shows n – type semiconductor at high temperature higher than 600 °C [53], also has large band gap (Eg ~ 4.9 eV) [54, 55]. Higher than 900 °C beta gallium oxide can detect oxygen gas only [56]. Nakagomi et al.

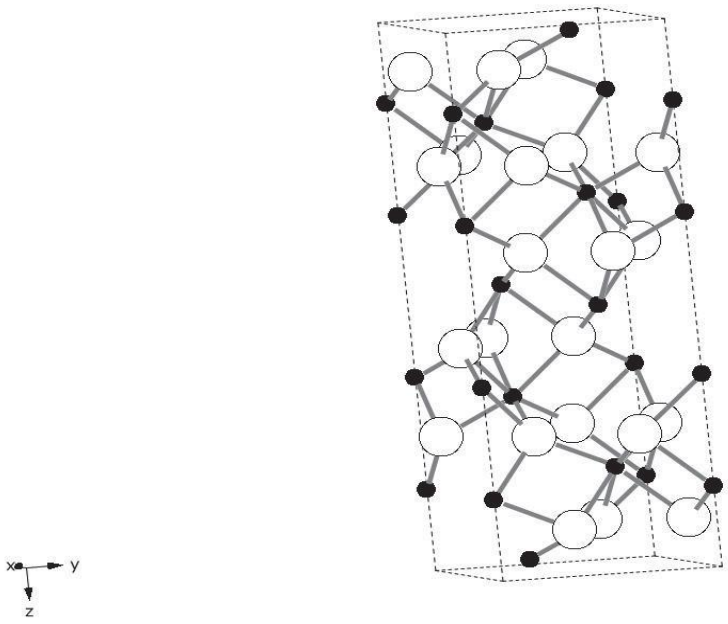

Figure 7: Corundum structure of β-Ga_2O_3. Filled-smaller and empty-bigger circles are Ga and O atoms

have fabricated and reported the ability of β-Ga_2O_3 single crystals toward hydrogen gas sensing at high temperature [57, 58]. Decomposition of organic pollutant, ultraviolet photodetector and photoelectrochemical water splitting with slight improvement are interested application of gallium oxide.

2.1.5 Zinc Oxide/Gallium Oxide Hetero-structure:

With increasing demand of current applications, there is a quick growth in improving new approaches for generating nanostructure with different and enhanced properties. The properties of the materials can be enhanced by formation of hetero-structure, doping and formation of core-shell structure. These approaches can provide new and inevitable properties for materials. As a result, lately many efforts have been concentrated in improving and creating new methods for preparation of materials in nanoscale, such as ZnO, SnO_2 and Ga_2O_3. These new hetero-structured materials have

several current utilization and application for example as a gas sensors, solar cell, optoelectronic and near UV-laser [59, 30]. Many semiconductors for instance $SrTiO_3$ and TiO_2 have been mentioned as a photoanode to generate hydrogen (H_2) and oxygen (O_2) from water with assistance of ultraviolet (UV) light [59,30]. On the other hand a portion of less than 5% of the overall solar energy that irradiates earth coming from UV photons. More than 45% of the solar spectrum lies in visible region, thus these require to design materials which absorb visible spectrum. Despite the utilization of the visible portion of solar energy is crucial for enhancing the semiconductors activity in solar cell application.

There are little semiconductors which have stability to achieve complete water splitting with assistance of visible light and in the absence of external potential. It is easy to prepare materials with desired band gap more than 1.23 eV and less than 3 eV that can response to visible portion of solar spectrum, $RbPb_2Nb_3O_{10}$ is the one of the favorable semiconducting materials toward overall water splitting due to its desired band gap 2.9 eV. But, all semiconductors that response to visible light suffer from ability to achieve reduction or oxidation of water [60]. For instance WO_3 can generate oxygen via water oxidation mechanism but it cannot reduce hydrogen ion (H^+) to produce hydrogen gas [61]. It is difficult to prepare materials to perform complete water splitting reaction, because the high electronegativity of O^{2-} anion that led to similar O 2p valence band edge situation 1.5 eV in absolute energy, which is less than minimally required to achieve water oxidation. In addition to the thermodynamic potential require 1.23 eV for water splitting with the similar required for over-potential of 0.3 eV to perform water oxidation, many of the proper semiconducting oxides will lose their ability for complete water splitting reaction even with proper distance between conduction and valence band that

can harvest the visible light with high efficiency. However, nitrogen is lower in electronegativity than oxygen (3.5 vs 3 for nitrogen in pauling scale). As a result, valence band energies will increase for oxynitride or nitride and other similar semiconductors oxides, permitting the potential for overall water splitting under visible light irradiation with concern of excellent stability of that semiconductor oxides frequently may show in strong redox conditions. Lately, several favorable oxynitride and nitride materials for water dissociation reaction have been emerged. TaON (Eg = 2.5 eV) and Ta_3N_5 (Eg = 2.1 eV) have illustrated as eligible materials for water oxidation with logical stability and quantum efficiency [62].

Extra study is require to prove the capability of this visible responsive oxynitride $LaTiO_2N$ with Eg = 2.2 eV toward overall water dissociation reaction, because it has been mentioned as excellent candidates for hydrogen and oxygen generation in a proper sacrificial agent [63, 64]. Wurtzite – type $(GaN)_1 - x\ (ZnO)_x$ semiconductor which is excellent materials known to date as photoanodes for total water splitting under visible irradiation, with quantum efficiency up to 6 % [65]. UV-responsive materials showed higher quantum efficiency with more than 60 % [66], thus there is no clear argument about visible responsive semiconductor did not reach this point, and by modifying and improving the electronic structured and optical properties of wurtzite $(GaN)_1 - x(ZnO)_x$ quantum efficiency will be enhanced. Both semiconductors ZnO and GaN with (Eg = 3.2 eV, 3.4 eV) recognized as wider band gap that are basically not response to visible energy. These materials are highly stable in the wurtzite form with space group $P6_3mc$, #186), and almost have identical lattice condition (GaN: a = 3.189 c = 5.185; ZnO: a = 3.249 c = 5.207). It was mentioned earlier this semiconductor $(GaN)_1 - x\ (ZnO)_x$ can

make solid solution with ability to response to visible irradiation and form electron – hole pair for both half reaction of water. Band gap of this materials $(GaN)_1 – x(ZnO)x$ it can decrease up to 2.4 eV [67] and that suggestion was confirmed by absorption edge observation. In addition theoretical calculations based on (DFT) which is density function theory for quasirandom structure proposed the band gap of this materials can decreased up to 2.29 eV with zinc amount of x = 0.525 [68,69]. More lately Monte Carlo simulation is confirmed that suggestion based on theoretical calculation [70].

2.2 Tungsten Oxide/Bismuth Vanadium Oxide for Water Splitting:

2.2.1 Tungsten Oxide Nanostructure:

Since 1970s WO_3 has been studied as hydrogen generation catalytic materials [71]. But the ability of tungsten trioxide to produce hydrogen is limited because of three different reason. Firstly, conduction band is not negative enough for reduction of hydrogen; secondly, tungsten trioxide is just stable in acid media; thirdly, band gap of WO_3 is relatively large 2.65 eV [72, 73]. Synthesis of tungsten trioxide on polyethylene glycol (PEG) was published lately [74]. WO_3 films recorded IPCE values of ~30 % in presence of assisted film and ~3 – 4 % in absence of PEG. During the preparation the thickness of PEG assisted film increased and this led to enhancement in IPCE value. Grimes et al. synthesized vertically aligned nanoarrays that improved the IPCE at 400 nm to 60 % [75] in contrast with randomly structured tungsten trioxide. Doping of anion in the tungsten trioxide lattice can enhance the catalytic activity. High amount of nitrogen – doping reduce the crystallinity of materials as a result this showed negative impact on photoelectrochemical activity of this materials [76]. The photocurrent raised with

nitrogen amount from 2.96 to 5.93 mA/cm^2 [77] because the significant decreasing in band gap from 2.52 to 1.89 eV, this is nitrogen - doped sample synthesized via reactive RF magnetron sputtering with N_2 gas. Glucose was inserted into spray precursor solution during the preparation of thin films of carbon – doped via spray pyrolysis method.

The band gap of these materials was reduced slightly from 2.62 to 2.57 eV however the photocurrent enhanced from 1.1 up to 1.6 mA/cm^2 [78]. Visible light responding enhanced to the overall photocurrent ~ 50 % because of the carbon doping. In the presence of methanol, the overall photocurrent can reach 2.6 mA/cm^2. Formation of stable semiconductor in higher pH by addition of copper is another possibility. Bartlett et al. prepared $CuWO_4$ thin films via electrodeposition approach which maintained pH values around 7 for long time of irradiation and decreasing band gap from 2.7 to 2.25 eV as well [73]. Al – Jassim and turner et al reported amorphous copper: tungsten films showed tunable band gaps, by changing the ratio of W: Cu the films were unstable in aqueous solution and result were not impressive for solar hydrogen conversion [79].

2.2.2 Crystal Structure of Tungsten Oxide:

Tungsten trioxide (WO_3), which is an n – type semiconductor, it has many use in technology for example photoelectrochemical water splitting, sensors and smart windows etc. [80-82] Production of photocurrent, band gap desirability and responding to solar energy are the properties required in photocatalytic materials [83, 84]. Moreover Tungsten trioxide has excellent stability versus photo-corrosion, higher photoresponse and high electron transfer character [85-89]. Monoclinic WO_3 crystal structure has superior Photoelectrochemical water splitting activity to other crystals structure of WO_3. Reaction mechanism and active sites of interaction at surface of the catalysis in

photoelectrochemical reaction of tungsten trioxide are not elaborated up to now. A series of polymorphs can be found for the bulk tungsten trioxide based on temperature and pressure, such as orthorhombic [90], γ- monoclinic [91], triclinic [92], tetragonal [93], and ε-monoclinic [94] structure. γ-monoclinic (WO_3) structure it is stable structure at room temperature, which can be visualized as a distorted 2 x 2 x 2 superstructure of the simple cubic ReO_3-type unit cell [95], by moving the WO_6 octahedra and replacing the central W atom. Bond length are almost identical along the [100] direction in that structure, thus other short – long bond presence along both [001] and [010] direction [96]. This anti-ferroelectric distortion guide to accumulate the crystal in the [001] direction, as a result the thin films produced by cleaving single crystals [97, 98]. Many practical efforts have been focused on WO_3 surface structure by low energy electron diffraction (LEED) and scanning tunneling microscopy (STM) methods, etc. [99-108].

Tungsten trioxide (001) and (100) thin films have been practically synthesized and many types of surface modification were carried out based on growth parameters. The γ-monoclinic WO_3 with surface (001) has the minimum energy, [105] as a result is breaking plane, which in principle can be finished either via O plane or WO_2 plane. In order to cancel electrostatic dipole tungsten trioxide thin films try to lose O_2 in the surface. For instance, ($\sqrt{2} \times \sqrt{2}$) R45° modification of the (001) surface can be achieved by removing of monolayer of the oxygen atoms alternatively along the [010] and [100] directions, as is clear in figure (8), in accordance with a periodicity $\sqrt{2}$ times that of the underlying like ReO_3 simple cubic frame-work. Based on theoretical studies many research have been mentioned the role of tungsten trioxide surfaces. Oliver et al. investigated the surface energies of the (111), (110) and 5 modifications of (001) surface

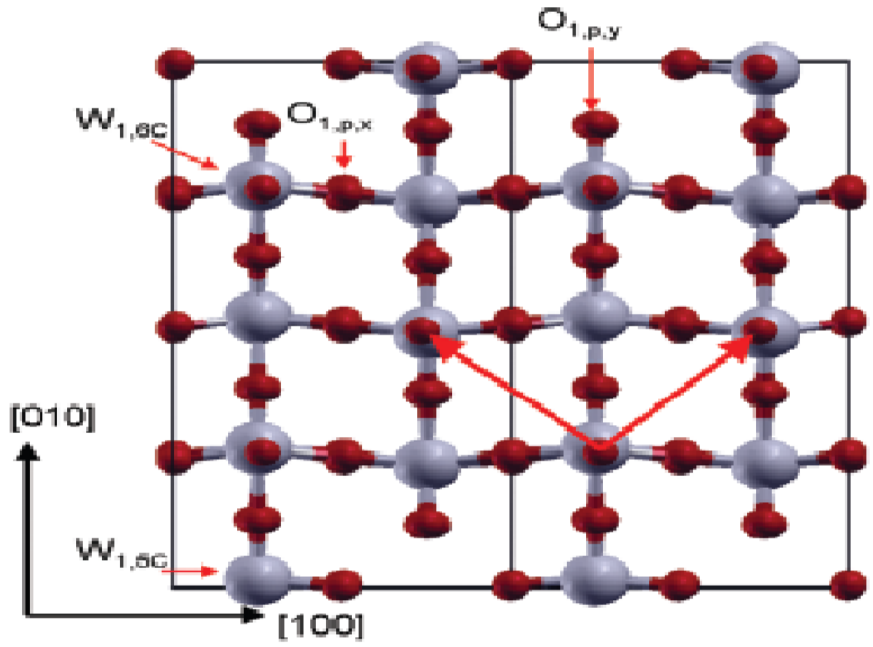

Figure 8: atomic structure of ((√2 × √2) R45 reconstruction of the (001) surface of γ-monoclinic WO_3.

of the idealized cubic tungsten trioxide, [109] and they noticed (√2 × √2) R45° modification of the (001) surface is the most stable because it has lowest surface energy. Valdes and Kroes et al studied the photooxidation of water on the (020), (002) and (200) surfaces of WO_3 in γ-monoclinic phase by applying density function theory approach [110].

2.2.3 Bismuth Vanadium Nanostructure:

Bismuth vanadate has narrow band gap energy 2.4 eV it response to solar energy in particular visible region [111]. Generally it is inexpensive, environmental benign and it can be prepared by facile approaches. In addition of high stability, photo-corrosion resistant and it response to solar energy conversion. Sayama et al synthesized thin film of

$BiVO_4$ on FTO substrate transparent electrode by metal organic decomposition approach [112] with enhanced interaction between FTO substrate and thin films. Lately, Grimes mentioned that the PEC behavior of bismuth vanadate could be enhanced by preparation of different structure of bismuth vanadate such as nanopyramids [113]. They also reported PEC water dissociation by $BiVO_4$ electrode which can be affected by the interaction between FTO probed with different size of $BiVO_4$ and photocatalysis [114].

The rule of thin films photoanode in PEC application, as a common pure bismuth vanadate decrease rapidly due to higher charge carrier recombination rate. When the photo-generated electron move randomly through the particle that introduce them to more recombination points and grain boundaries before their collection at the surface of the electrode. This behavior can be obtain in the new photocurrent formed in the pure film of bismuth vanadate. Kisch et al mentioned that bismuth vanadate with p-type cobalt oxide can generate a p – n junction to enhance the charge separation efficiency [115]. Sayama and his co - worker again demonstrated that treating of bismuth vanadate by Ag ion can improve the responding of visible energy and produce photocurrent as ~ three times order [116]. Lately park et al investigated the potential status of bismuth vanadate photoelectrode [118], in utilizing in tandem water dissociation, $BiVO_4$ either in equivalent nanostructured or thin film it has to be contacted electrically. Solution phase chemistry coupled with spray pyrolysis or spin coating are the common approach of preparation bismuth vanadate film [118 – 121]. Electrochemical deposition has been mentioned as well. The highest photocurrent recoded theoretically at 2.4 eV is 7.5 mA/cm^2, unimproved bismuth vanadate recoded less than 1 mA/cm^2 [122, 123,124] as a photocurrent for water splitting under AM1.5 condition, which is less than the

theoretically obtained. $BiVO_4$ has disadvantage such as slow kinetics of water oxidation and poor electron transfer this proved by higher photocurrent of back versus front illumination [125,126]. Co – catalysis doping such as Co – Pi and hole – scavenging of back contact can enhance the activity dramatically [120, 121, 127]. Several metal nitride and oxide thin film such as $BiVO_4$, TaON and ZnO used as photoanode in PEC process [128 - 130] were prepared by scalable and commercially available sputtering system. Preparation of bismuth vanadate thin film by physical vapor deposition approach was demonstrated relatively late [124, 131].

2.2.4 Crystal Structure of Bismuth Vanadate:

Bismuth vanadate can be found in 3 polymorphs crystal structure, dreyerite, clinobisvanite and pucherite. Pucherite discovered in nature in form of $BiVO_4$ it has orthorhombic crystal structure (space group *Pnca* with a = 5.332 Å, b = 5.06 Å and c = 12.02 Å) [132], and crystal was named according to place where it found (Pucher Shaft, Wolfgang Maaβen mine field, Schneeberg, Germany). Bismuth vanadate synthesized in the laboratory, in general don't have pucherite structure. clinobisvanite has a monoclinic (scheelite-type) crystal structure (space group C_2/c with a = 7.247 Å, b = 11.697 Å, c = 5.09 Å and β = 134.226^o) [133, 134]. While Dreyerite has a tetragonal (zircon-type) crystal structure (space group $I4_1/amd$ with $a = b$ = 7.303 Å and c = 6.584 Å), [135] Figure (9) shows these different crystal structures for $BiVO_4$. A scheelite-type tetragonal crystal structure also exists, which is a slight modification of the monoclinic clinobisvanite $BiVO_4$ in terms of the atomic positions of Bi, V, and O (space group $I4_1/a$ with $a = b$ = 5.147 Å, and c = 11.7216 Å) [133]. Each bismuth ion is linked by eight oxygen atoms (dodecahedral), and every vanadium in all bismuth vanadate ion is linked

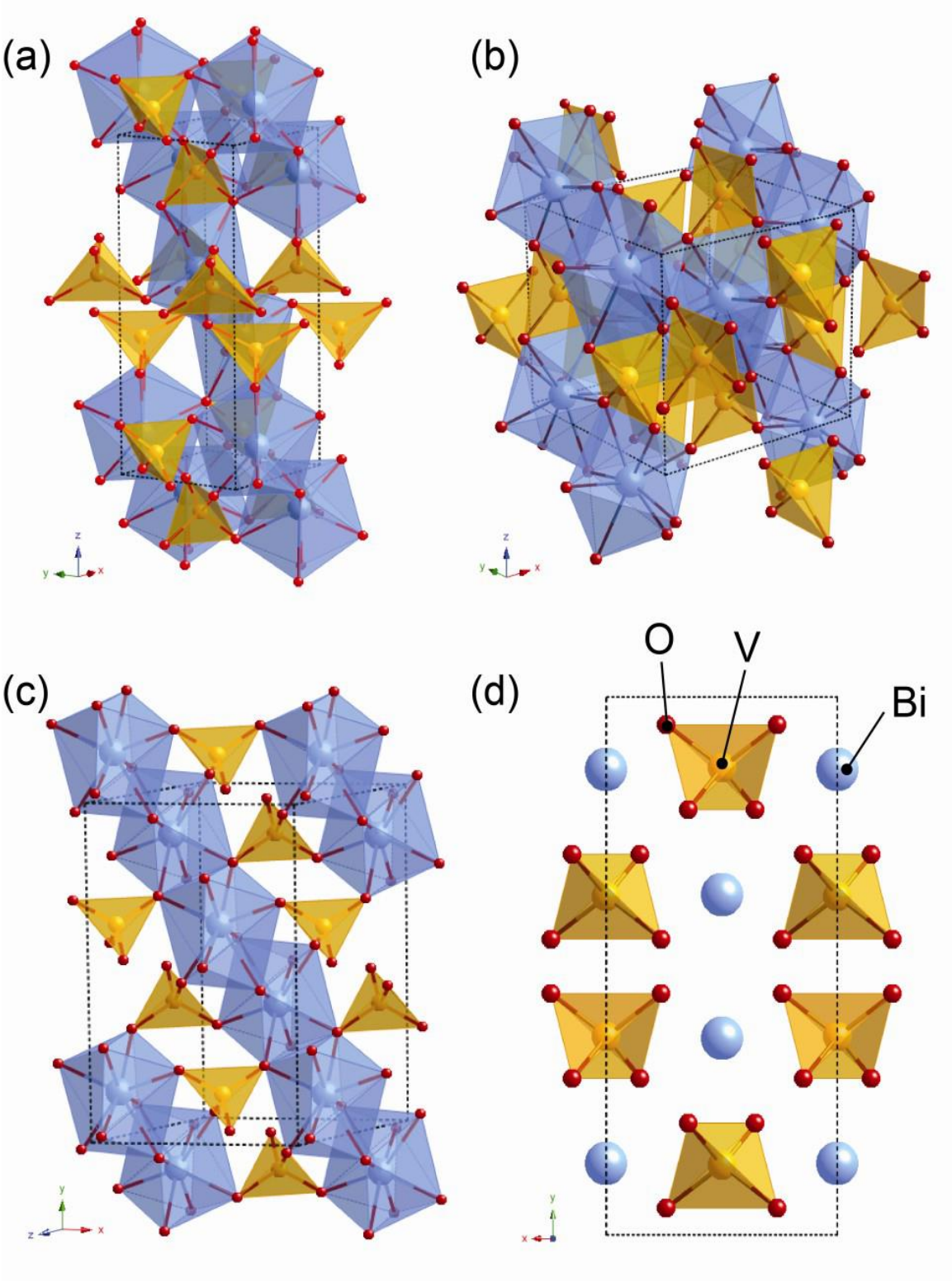

Figure 9: Crystal structure of different $BiVO_4$ polymorphs: (a) pucherite (orthorhombic), (b) dreverite (tetragonal zircon), (c) clinobisvanitee (monoclinic sheelite), and the side view (c axis) of the clinobisvanitee structure is shown in (d).

by four oxygen atoms (tetrahedral). In the scheelite structure, every BiO_8 dodecahedral unit is surrounded by various eight VO_4 units. Every oxygen atom is linked to one vanadium center and two bismuth centers. This is correct for tetragonal scheelite and monoclinic structure. But there is distortion in the monoclinic scheetile in the local environments of bismuth and vanadium ions is noticed. Therefore the 4 – fold symmetry is lost. It can be viewed from the different in bond angles between these two structures, as shown in Table (1). In a tetragonal scheetile all four vanadium – oxygen bond lengths are similar (1.73 Å), and only 2 differences in bismuth – oxygen bond lengths recorded (2.4 and 2.47 Å) [133]. In contrast in the monoclinic scheetile structure there are 4 – differences in bismuth – oxygen bond lengths (2.52, 2.35, 2.63 and 2.37 Å) and 2 – differences in vanadium – oxygen bond lengths (1.76 and 1.69 Å). This distortion in the monoclinic is supposed to be responsible for excellent photocatalytic process in comparing with tetragonal scheetile structure, as reported by Tokunaga et al [136]. This distortion improve the local polarization which enhance the electron – hole separation, in photoelectrochemical processes.

Table 1: Bond lengths of Bi – O and V – O in different crystal structure of $BiVO_4$

Bond	Bond Length (Å)			
	Monoclinic Scheetile	Orthormbic	Tetragonal Zircon	Tetragonal Scheetile
V – O	1.76 1.69	1.7	1.7	1.95 1.76
Bi – O	2.35 2.52 2.63 2.37	2.2 2.53 2.73 2.31	2.55 2.41	2.47 2.4

In the zircon type structure two VO_4 units offer two oxygen atom and 4 VO_4 units offer one oxygen atom to bismuth. In addition every BiO_8 dodecahedral unit is surrounded only by six VO_4 tetrahedral units. Eventually in the orthorhombic type structure, every BiO_8 units is surrounded by seven VO_4 units since one VO_4 units provide two oxygen atom to bismuth atom. The bond lengths of these two crystal structure is summarized in table 2.1. The monoclinic structure is normally formed via high temperature preparation approach, while the zircon structure in general produced via low temperature preparation methods, for example aqueous precipitation at room temperature [111, 137]. The tetragonal scheetile phase is produced by higher temperature in comparison with monoclinic scheetile. The zircon structure can transformed irreversibly to monoclinic scheetile at ~ 400 – 500 °C [111, 138].

2.2.5 Tungsten/Bismuth Vanadium Hetero-structure:

Metal oxides photoelectrodes have been studied long time ago, more emphasis has been given to ternary metal oxides. However only few of them showed promising photocatalytic properties [138,139], and still they do not cover all requirements for photoelectrochemical water splitting. Thus the improvement of much complicated metal oxides such as ternary metal oxides, can be carried out to improve overall properties. Bismuth vanadate $BiVO_4$ is one of the most promising binary metal oxide photoanodes for photoelectrochemical water splitting because of it is narrow band gap appromx 2.4 eV, (in the monoclinic phase), inexpensive, highly stable and resistant to photo-corrosion. Based on theory solar to hydrogen (STH) conversion efficiency of $BiVO_4$ approaches 9.2% with the highest photocurrent of ~7.5 mA/cm^2 for solar light illumination (100 mW/cm^2) under standard air mass 1.5 condition [140] because the recombination of

photo-generated holes and electron. $BiVO_4$ has poor electron transport properties that hinder the kinetics of water splitting reaction. To improve the transport efficiency of $BiVO_4$ many approaches have been applied such as doping with Mo [141-143] or W [144,145] gave a restricted result. Generation of hetero-junction $BiVO_4$ core-shell in three dimension nanostructured with other excellent conductive semiconducting oxides is a favorable way to improve transport properties of $BiVO_4$.

The thickness of $BiVO_4$ absorber layer dramatically contribute in the enhancement collection of photo-generated carriers, prior to separation. In contrast the optical thickness of the absorber is reformed by offering excellent structured arrangement. The optical path through the devices was increased at the nanostructured interfaces of light scattering and therefore the photon absorption was drastically improved. Therefore the photocurrent in the photoanode can reach it maximum value via optimization of separate electronic and optical thickness of the $BiVO_4$ absorber, the reversible connection between short lifetime and light absorption efficiency of the photo-generated carriers is decreased. Much work was carried out on $BiVO_4$ hetero-junction with $CuWO_4$ [146] and WO_3 [147, 148, 149] are available, but they were synthesized mainly in the two-dimension arrangement plain which does not overcome the reversible dependence of the electron lifetime and light absorption as in three dimension core-shell structure. The previous photoanodes were fabricated by various technique, in two step of deposition that leads to generate recombination points and trapping at the hetero-junction interface. Moreover spin coating deposition of $BiVO_4$ resulted in covering total gaps between the WO_3 –NRs, which is mainly decreased the advantage of the electronically thin $BiVO_4$ absorber. Only Su et al. [147] mentioned the preparation of WO_3 –NRs/$BiVO_4$ hetero-junction

photoanodes, the WO_3-NRs/$BiVO_4$ fabricated via solvothermal deposition approach were not well-aligned. However WO_3/$BiVO_4$ nanostructured photoanode exhibited enhanced IPCE value that jumped from 9.3% to 31% comparing to WO_3/$BiVO_4$ planar hetero-junction prepared by same approach, and resulted in photocurrent of 0.8 mA/cm^2 at 1.23V reversible hydrogen electron (RHE) [147]. Saito et al. [148] investigated recently a photocurrent of 2.8 mA/cm^2 at 1.23V RHE in a single hetero-junction WO_3/$BiVO_4$ photoanode with planar thin film arrangement. Gradually increase in photocurrent to 3.04 mA/cm^2 at 1.23V RHE is carried out by the incorporation of SnO_2 structure and generate WO_3/SnO_2/$BiVO_4$ photoanode, where SnO_2 act as blocking layer. The photocurrent was gained in $KHCO_3$ potassium hydrocarbonate electrolyte, which raised the question about the role of $KHCO_3$ as sacrificial agent. WO_3 /SnO_2 /$BiVO_4$ photoanode resulted only 1.1 mA/cm^2 in stable 0.5 M Na_2SO_4 (PH=7) electrolyte. Van de krol et al. [150] mentioned a photocurrent of 4 and 3 mA/ cm^2 in the $BiVO_4$ photoanode doped by W in double and single-junction respectively coupled with Si solar cell. However the photocurrent were recorded in a mixture of di and monobasic hydrophosphate K_2HPO_4 and KH_2PO_4 which are the compositions of potassium buffer solution 0.1 M. Kitamori et al. illustrated WO_3/$BiVO_4$ nanostructured photoanode well-aligned and excellent separated WO_3 nanorods capped with deeply thin $BiVO_4$ absorber layer with photocurrent of 3.2 mA/cm^2 in 1.23 V RHE gained in stabilized 0.5 M Na_2SO_4 (PH = 7) electrolyte under simulated AM 1.5 solar light. They fabricated ITO /WO_3-NRs /$BiVO_4$ photoanode structure through the set of normal regimes multi-magnetron sputtering and r.f. reactive magnetron sputtering in Glancing Angle Deposition (GLAD).The photocurrent was improved

because the rapid charge isolation in the electronically thin $BiVO_4$ absorber layer that dramatically decreased the recombination of charge.

The morphology of WO_3/NRs/$BiVO_4$ nanostructured contribute in light trapping that reformed the impact of optical thickness of the $BiVO_4$ light absorber. The IPCE spectra showed that the photocurrent resulted in optimized photoanode is gained from little participation of WO_3 nanorods and major contribution of the $BiVO_4$ absorber thin layer. Their outcomes explain the idea of using highly thin light absorber layer, that offer a favorable pathway for enhanced photocatalytic approach in terms of hydrogen production through water splitting. In this study, we mentioned development in method of fabricating hetero-structured WO_3/$BiVO_4$ photoanode on indium oxide tin oxide ITO substrate in two step of fabrication, the first step is the growth of tungsten seeds using sputtering system, then followed by hydrothermal growth of WO_3/$BiVO_4$.

CHAPTER 3

Synthesis and Fabrication of Zinc Oxide/Gallium Oxide Photoanode

3.1 Experimental Work:

3.1.1 Fabrication of Zinc Oxide Seeds:

Zinc oxide seeds were fabricated by physical approach using automatic sputter coater on indium oxide tin oxide glass coated substrate (ITO). The deposition was carried out using base pressure of 9.1 x 10^{-6} Pa and working pressure was 5 x10^{-3} Pa, the duration of deposition was 40 min using 80 W power.

3.1.2 Fabrication of Zinc Oxide/Gallium Oxide Hetero-structure:

Thin films of ZnO/Ga_2O_3 hetero-structured was synthesized by hydrothermal approach as in literature [151]. Precursor solution of zinc oxide was prepared by mixing 0.03 M from Zn $(NO_3)_2.6H_2O$ (99.78 %, Fisher Scientific) in deionized (DI) water and 4 M of hexamethylenetetramine (HMT) (99.5 %, Sigma Aldrich).

Hetero-structured ZnO/ Ga_2O_3 thin films were synthesized and fabricated on ITO (0.5 cm X 1.5 cm) substrate (Indium oxide Tin oxide – glass coated), by adding 0.5%, 2 %, 5 % of gallium (III) acetyl acetone (99.99 %, Sigma Aldrich) respectively to the precursor solution of ZnO. These solution mixture has been transferred to a Teflon vessel, sealed in an autoclave and maintained in an oven at 90 °C for 6 hours. Then the substrate were removed from an autoclave, washed with DI water and annealed at 450 °C

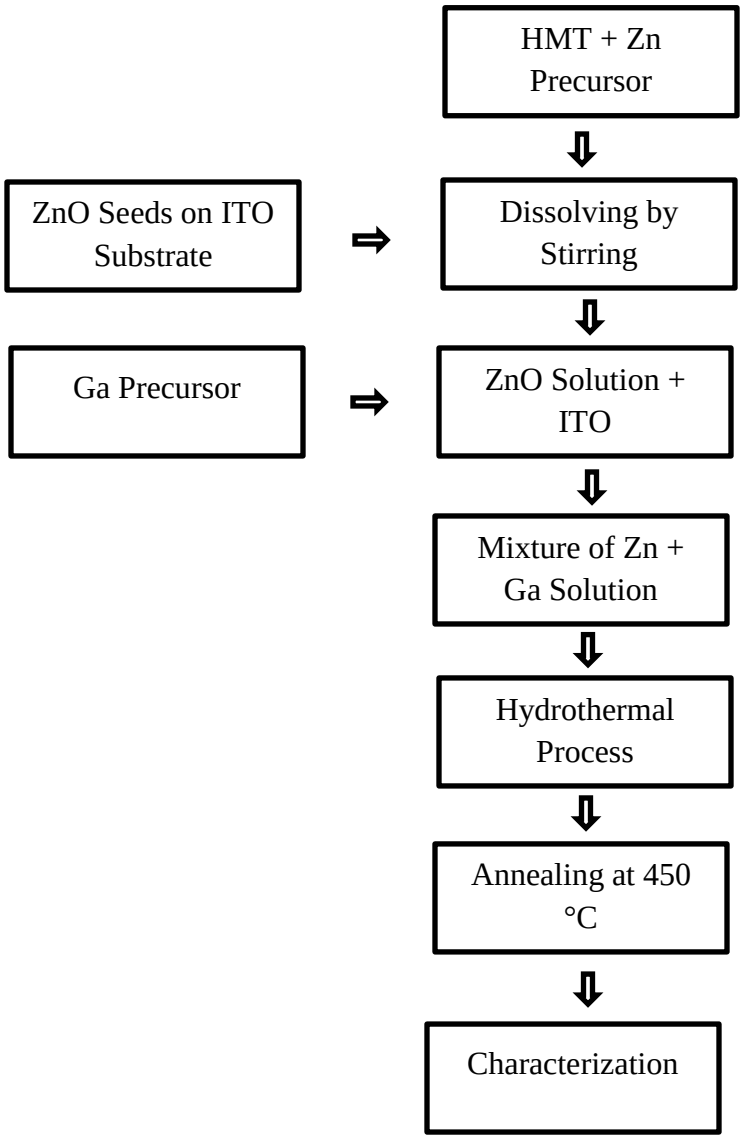

Figure 10: Schematic illustration of ZnO/Ga_2O_3 thin film fabrication

for 2 hours. The synthesis and fabrication process are illustrated in figure (10).

3.1.3 Characterization:

3.1.3.1 XRD and Raman Spectroscopy:

The crystalline hetero-structure was characterized by powder X – Ray Diffractometer rigaku rint – 2500. Radiation: Cu Ka lamb: 1.54060, λ = 1.54056 A, the

range was between 10 – 60 in 2 θ degree and scan rate was 3 sec. Powder samples and thin film was placed on the glass plate.

The Raman analysis were performed at room temperature using Yvon Jobin Horiba Raman spectrometer (iHR 320) model with charge coupled detector (CCD). The laser source was green type at 532 nm line and intensity was 45 %. The spectrums were obtained from the scattered light normal to the sample surface, with grating position 600 mm, slit width 96 cm, accumulation number was 3 and exposure time 10 sec.

3.1.3.2 FESEM and EDS Analysis:

The morphological properties of these materials were analyzed by field emission scanning electron microscope FESEM - TESCAN – LYRA - 3 and elemental mapping (EDS) of these materials were investigated by the oxford instrument coupled with FESEM. Powder samples and thin film were mounted on sample holder using double sided copper conductive tape.

3.1.3.3 Optical Measurements:

Room temperature photoluminescence was carried out with a xenon lamp associated with a frequency doubling system operating at 380 nm as the excitation source with an integration time 0.1 sec in the range from 400 nm to 730 nm using Yvon Jobin Horiba instrument model no FL3- 2iHR.

UV – VIS analysis was investigated at room temperature by Cary series UV – VIS – NIR spectrometer, (Agilent technology).

3.1.3.4 Photoelectrochemical (PEC) Set-up:

The photoelectrochemical measurements was investigated according to the standard photoelectrochemical work station [152]. Chronoamperometry (CA) and linear sweep

voltammetry potentiostatic (LSVP) were conducted using two electrode set-up, platinum wire and ZnO/Ga_2O_3 thin film as counter and working electrode respectively in 0.1 M potassium hydroxide (KOH) [PH = 13] electrolyte. Metrohm autolab (B.V) Potentiostat / Galvanostat PGSTAT 10 was used to investigate the photocurrent at a scan rate of 0.0999 V/sec, coupled with oriel sol 3A class AAA solar simulator 100 mW/cm^2 and AM 1.5 filter (1 sun, Oriel) as a source of illumination. All photoelectrochemical analysis are explaining here according to the normal hydrogen electrode (NHE).

3.2 Results and Discussion:

3.2.1 Formation of Zinc Oxide Seeds:

ZnO seeds were deposited on the ITO substrate using automatic sputter coater as physical approach. As in Figure (11 a) which is illustrating powder XRD of bare ITO and ZnO seeds, it is clear that the entire substrate has been covered by ZnO seeds because all ITO diffraction peaks have been disappeared totally, only (114), (111) and (220) corresponding to wurtzite hexagonal ZnO appears at 31.42, 36.36 and 61.26 in 2 θ degree respectively (JCPDS#: 01-077-9355). The morphology of seeds layer have been investigated by FESEM – TESCAN and revealed the homogeneity of the seeds on the entire substrate with smooth surface and there is no grains observed. In addition the size of the seeds is extremely small. Thus it is difficult to discriminate between bare ITO and ZnO seeds by naked eye see Figure (11 b & c). Furthermore the compositional characterization has carried out by Oxford instrument coupled with FESEM and showed the presence of Zn and O atom as in Figure (11 d) and from quantitative analysis oxygen is more than zinc as it is expected see Figure (25 b) in appendix A.

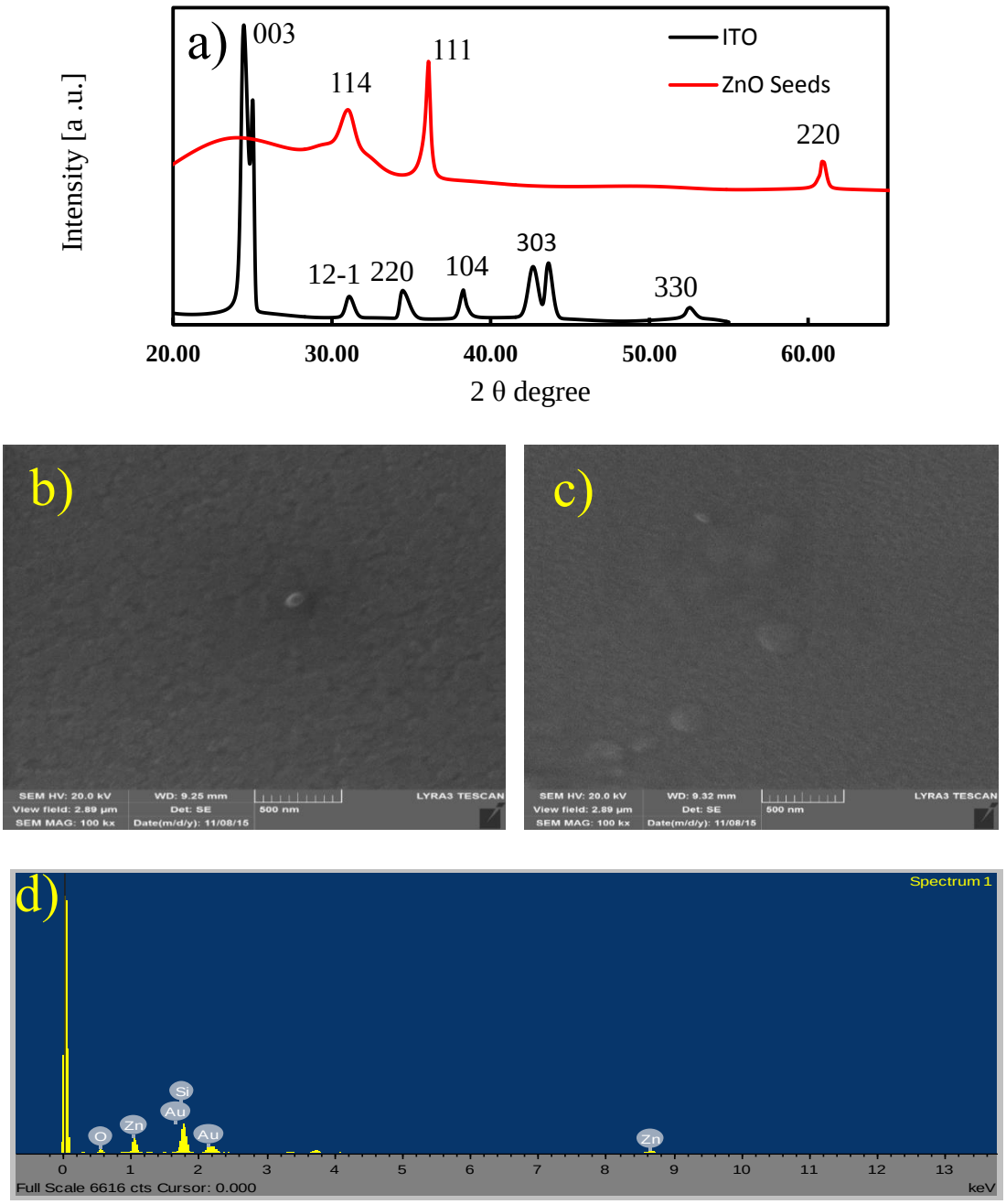

Figure 11: a) XRD of ITO and ZnO seeds, FESEM of b) bare ITO, c) ZnO seeds and d) EDS analysis of ZnO seeds

3.2.2 Fabrication of ZnO/Ga_2O_3 Hetero-structure:

ZnO/Ga_2O_3 hetero-structure nanorods were fabricated on ITO substrate by hydrothermal method on the fabricated ZnO seeds. Figure (12 a) shows the XRD pattern

of bare ITO, ZnO seeds and annealed ZnO/Ga_2O_3 nanorods. The ITO substrate has characteristic peaks at 29.62, 30.19, 37.59, 40.49, 44.47, 48.31, 48.95 and 57.80 in 2 θ degree which are corresponds to the (003), (12-1),(220), (104), (303), (042), (23-1) and (330) growth directions respectively and belong to ITO (JCPDS #: 01-077-8214). These peaks have been disappeared completely, covered by new peaks which are 31.42, 36.33 and 61.20 correspond to (114), (111) and (220) as a result of depositions of ZnO seeds (JCPDS #: 01-077-9355) in a wurtizte hexagonal phase. This indicate that the surface of the substrate has been covered by ZnO seeds layer which acts as nucleus centers on the surface of the substrate. Well-aligned ZnO/Ga_2O_3 nanorods have been grown hydrothermally in one step by direct immersion of ITO substrate in the precursor solution. The XRD pattern of annealed ZnO/Ga_2O_3 hetero-structure exhibit polycrystalline structure in orthorhombic crystal system (JCPDS #: 01-076-9637). The X – ray diffractions peaks correspond to (063), (114), (065), (0014) and (199) at 2 θ degree planes of 29.32, 31.41, 32.76, 51.59 and 61.20 respectively.

Raman measurements as in Figure (12 b) of pure ZnO and ZnO/Ga_2O_3 hetero-structure have been conducted at room temperature and revealed that the finger print of pure ZnO at 382 and 413 cm^{-1} are belong to the transverse optical A_1 (TO) and E_1 (TO) modes respectively. The highest peak at 438 cm^{-1} is correspond to the high frequency E_2 mode. The line around 589 cm^{-1} is correspond to the longitudinal optical mode (LO), and all these lines are diagnostic for hexagonal wurtzite structure for ZnO in an excellent agreement with literature [153-155]. With the addition of gallium oxide to ZnO structure there are some change were observed in the Raman spectrum of the hetero-structure metal oxides. The lines at 382 and 438 cm^{-1} remains similar, while the peaks at 413 cm^{-1}

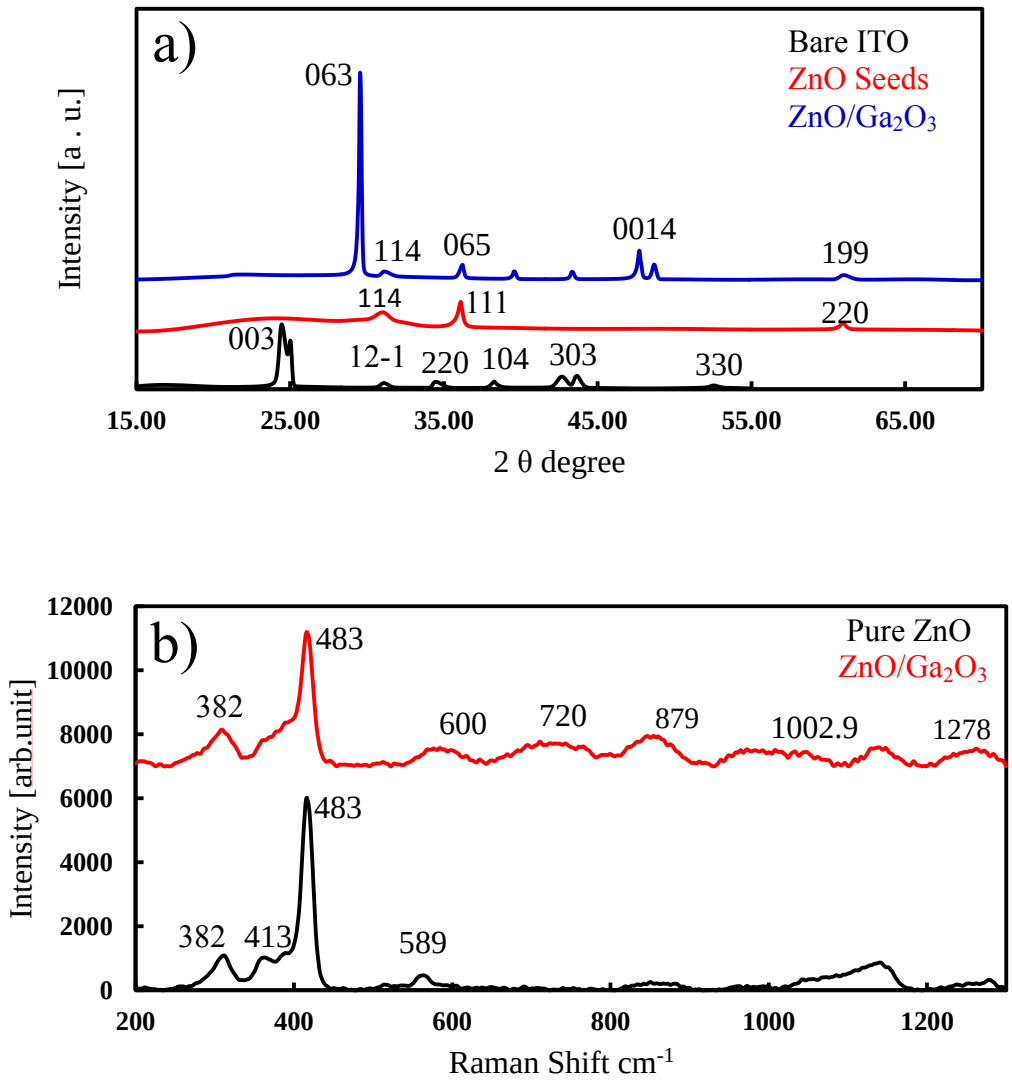

Figure 12: a) XRD and b) Raman spectrum of ZnO and ZnO/Ga_2O_3 thin film

disappeared completely and the shoulder at 571.8 cm^{-1} has been shifted and became broad, due to structural strain of hetero-structure. In addition to the appearances of new peaks such as 720, 879, 1002, 1278 cm^{-1}. These peaks are classified as group of (> 580 cm^{-1}) with medium intensities as Ag symmetry that are originated by the GaO_4 tetrahedra related optical phonons [156,157]. All these changing may explained as changing in the

crystal structure of ZnO with the introduction of GaO and formation of hetero-structure ZnO/Ga_2O_3.

The surface morphology of the annealed ZnO/Ga_2O_3 thin film were studied by (FESEM), TESCAN dual beam as in Figure (13 a & b) shows low and high magnification FESEM micrographs of ZnO/Ga_2O_3 NRs. Low magnification FESEM images revealed that low density nanoarrays are grown on the large scale ITO conducting substrate. Each nanorod is 500-600 nm in length and 40-50 nm in their diameter. High magnification image clearly demonstrates faceted hexagonal shape of each nanorods. These hetero-structured arrays are highly ordered and uniform. Generally, low and high magnification images reveal that these nanoarrays are dense, aligned and ordered on the

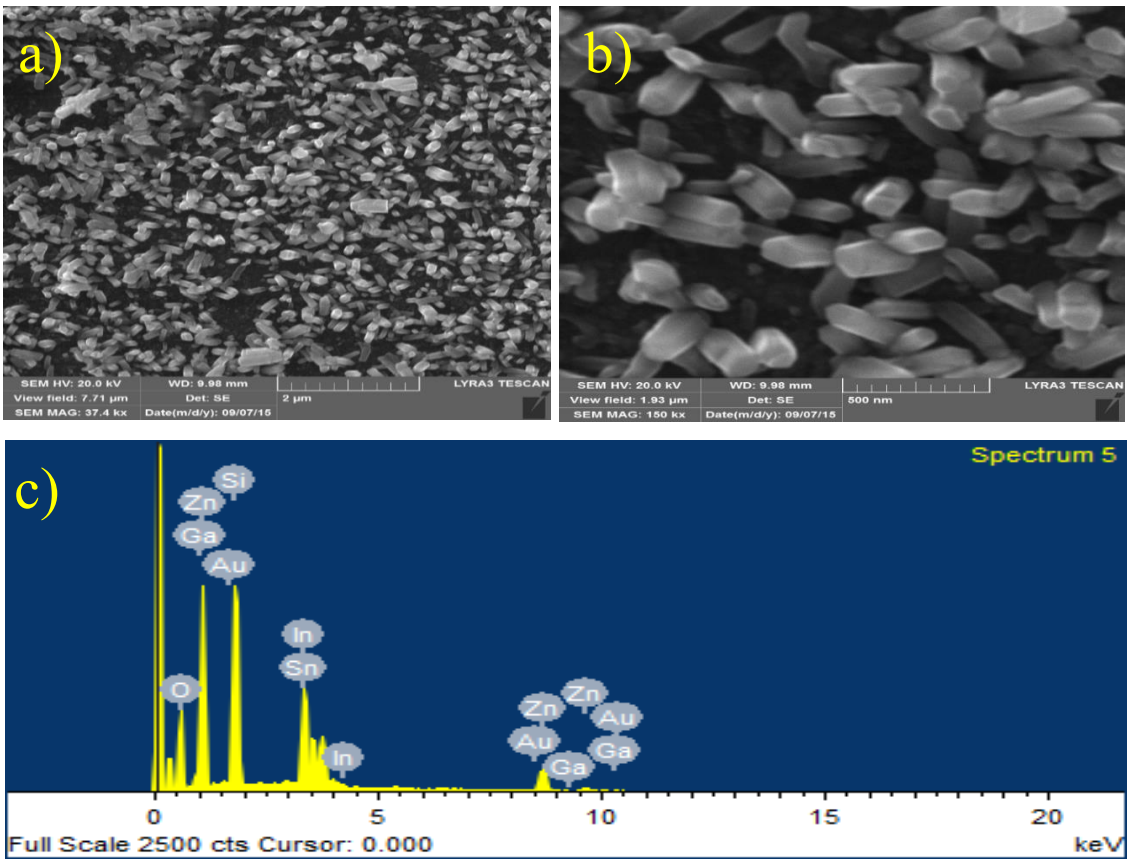

Figure 13: FESEM at a) low, b) high magnification and c) EDS analysis of ZnO/ Ga_2O_3

conducting substrate. Tilted images showed the alignment of the arrays. The energy dispersive x-ray electron spectroscopy (EDS) show that the presence of the Zn, Ga and oxygen in addition to the ITO component see Figure (13 c).

In the UV – VIS absorption spectra, the pure ZnO nanorods illustrate broad absorption edge with onset at 465 nm and this can be explained as near – band – edge (NBE) absorption of ZnO nanorods. With introduction of Ga_2O_3 to ZnO, the ZnO/Ga_2O_3 photoanode UV – VIS absorption spectra gave the same broad band with slight shift in UV – VIS onset and can be attributed to change in crystal structure of ZnO see figure (14 a) [158]. Furthermore, the diffuse reflectance spectra has been carried out to draw relation of Kubelka-Munk function F(R) with photon energy *hv* (eV) in the range (0 – 5 eV). $F(R) = (1 - R)^2/2R$ is the relation give Kubelka – Munk function, where R is the magnitude of reflectance [159]. The band gaps were determinate by extrapolating the linear part of $F(R)^2$ curve (y axis) until it intersects with x (axis) which is the energy (eV). Generally in the reflectance spectra low values of reflectance mean high absorption in the specific location of wavelength. The pure ZnO and ZnO/Ga_2O_3 thin film reported band gap of 3.02 and 2.96 eV respectively, which reflect the slight change of the UV – VIS spectra onset see Figure (14 b). Thus this mean the ZnO/Ga_2O_3 photoanode can harvest visible-region of solar energy. The room temperature photoluminescence spectra of pure ZnO and ZnO/Ga_2O_3 photoanode hetero-structure as in Figure (14 c). A broad peak at 604 nm refer to deep level emission (DL) [160,161]. This peak is due to the oxygen vacancies, zinc vacancies or zinc interstitials [159,162 -164]. The intensities of the peak is mainly depend on the presence of the Ga_2O_3. The intensity of broad peak of ZnO has been quenched with the incorporation of Ga_2O_3 to ZnO structure.

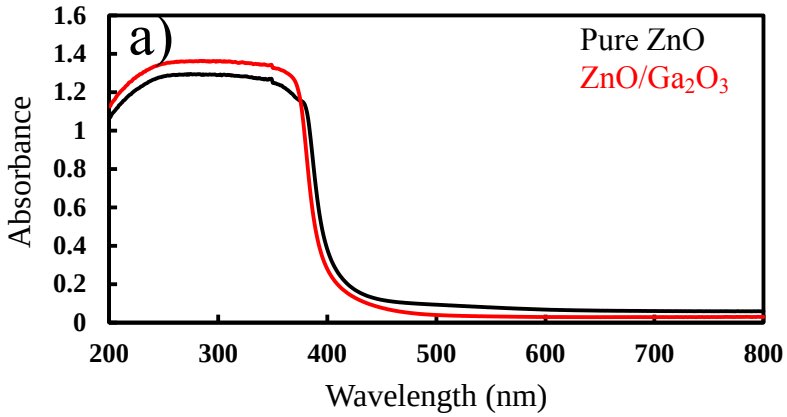

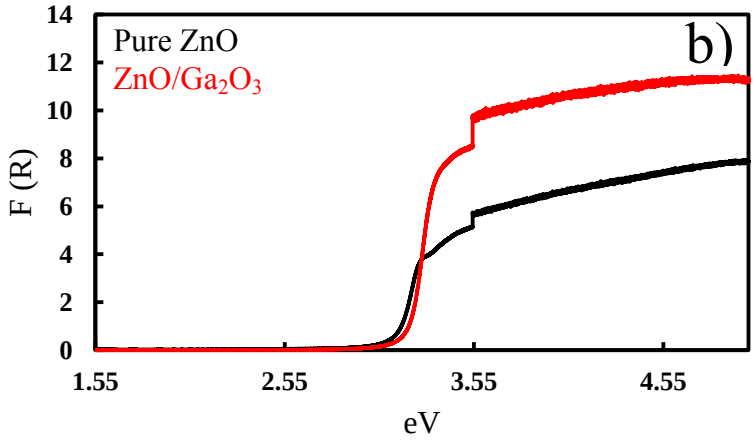

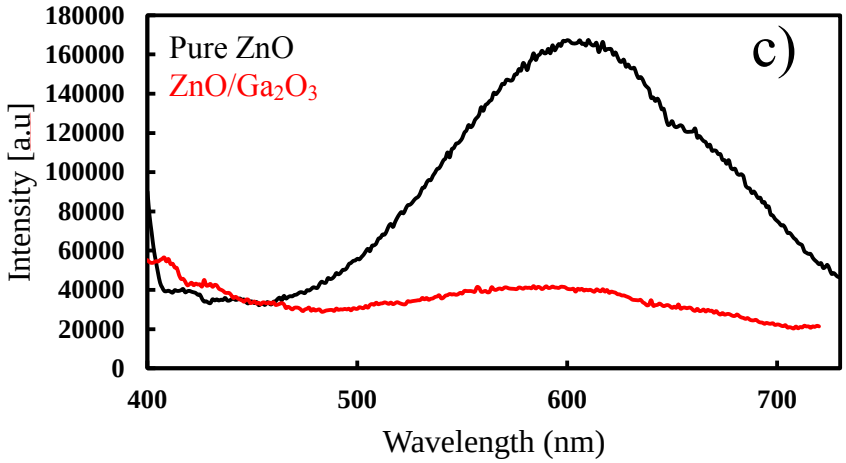

Figure 14: a) UV - VIS, b) Reflectance and c) PL spectrums of ZnO/Ga_2O_3 thin film

Table 2: UV – VIS onsets and band gap energies of ZnO and ZnO/Ga_2O_3 nanorods

Structure	UV – VIS Onset (nm)	Band gap (eV)
ZnO	410	3.03
ZnO/Ga_2O_3	420	2.96

3.2.3 Photoelectrochemical Properties:

The photoelectrochemical measurements of the ZnO/Ga_2O_3 photoanodes were investigated in two electrode set-up. Platinum wire and ZnO/Ga_2O_3 thin film as counter electrode and Working photoelectrode respectively in 0.5 M KOH [PH = ~13] as an electrolyte. Metrohm autolab (B.V) Potentiostat / Galvanostat PGSTAT 10 used as a potential source. Solar simulator class 3A (Oriel) was used as illumination source, the photoanodes were exposed to the front side illumination (through ITO) with 1.5 AM (1 sun) simulated solar class 3A (Oriel). Chronoamperometry measurements (*J* p) versus time (t) profiles were conducted with on and off illumination at 0.5 V versus platinum wire. As a result of light irradiation at 100 mW/cm^2 a spike in the photoresponse were noticed for three samples owing to the transient affect in power excitation, and the photocurrent then come back quickly to stable state. The photocurrent raised with the percent of the Ga_2O_3 gradually. As a result of loading gold (Au) on the ZnO/Ga_2O_3 nanorods photoanode the light absorption increase, assist the charge transport to the electrolyte/electrode interface and the ZnO/Ga_2O_3/Au NRs arrays photoanode recorded the highest photocurrent regarding-less to the Ga_2O_3 percent, and this can be refer to the surface plasmon resonance of Au nanoparticles see Figure (15) [165].

Linear sweep voltammetry potentiostatic (LSVP) has been carried out with previous set-up from 0 to 1.5 V versus normal hydrogen electrode (NHE) for further investigation of the thin film amount and the light effect. ZnO/Ga_2O_3 has been deposited on the (0.5 cm X 1.5 cm) ITO. ZnO/Ga_2O_3 photoanode was active toward oxygen evolution reaction (OER). It is evident that the photo-activity of photoanode depend on the Ga_2O_3 percent [166]. Water oxidation photocurrent onset began at 0.95 V versus (NHE), the current density increases gradually from 2 % to 5 % ZnO/Ga_2O_3 thin film and reached the maximum at 1.5 V which were 0.20 mA/cm^2 and 0.22 mA/cm^2 respectively. Similarly for ZnO/Ga_2O_3/Au (gold) coating photoanode the photocurrent increased significantly and recorded 0.36 mA/cm^2 at 1.5 V as maximum response in the dark. Thus, this is attributed to surface plasmon resonance of gold nanoparticles which were coated on ZnO/Ga_2O_3 NRs arrays surface, see Figure (16). When those photoanodes exposed to the light water

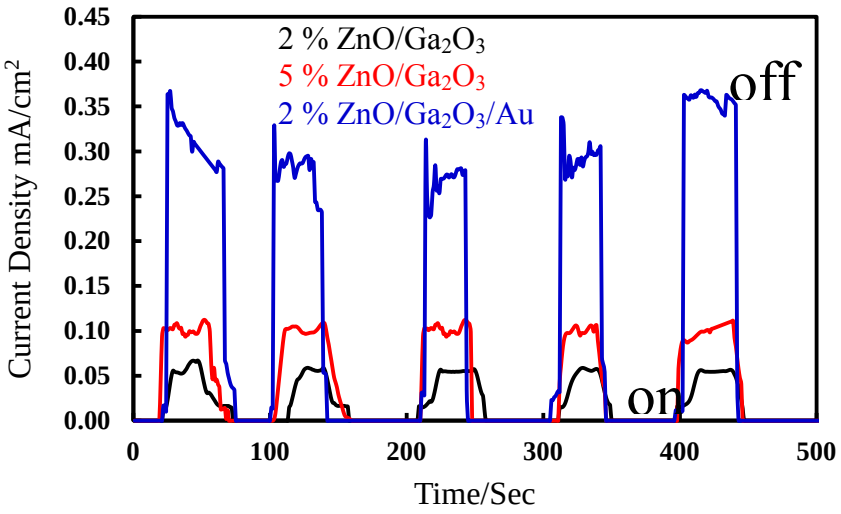

Figure 15: Chronoamperometry of 2 %, 5 % ZnO/Ga_2O_3 and 2% ZnO/Ga_2O_3/Au

oxidation onset began at 1 V and the photocurrent increased gradually until recorded the highest value 0.24 mA/cm^2 and 0.30 mA/cm^2 at 1.5 V for 2 %, 5 % ZnO/Ga_2O_3

respectively. Similarly, as consistent with previous results the 2 % ZnO/Ga_2O_3/Au thin film started water oxidation at low potential 0.86 V and recorded the highest photocurrent 0.60 mA/cm^2 this is due to the surface plasmon resonance of Au nanoparticles. Which is facilitate the charge transfer to the electrolyte/electrode interface by enhancing the absorption of the light see Figure (16). The effect of the light on the same percent was investigated as well. As it can be seen from Figure (31 a) in appendix A LSVP of 2 % ZnO/Ga_2O_3 the photoresponse enhanced when the thin film exposed to the light and recorded 0.24 mA/cm^2 compared to the dark 0.18 mA/cm^2 at 1.5 V.

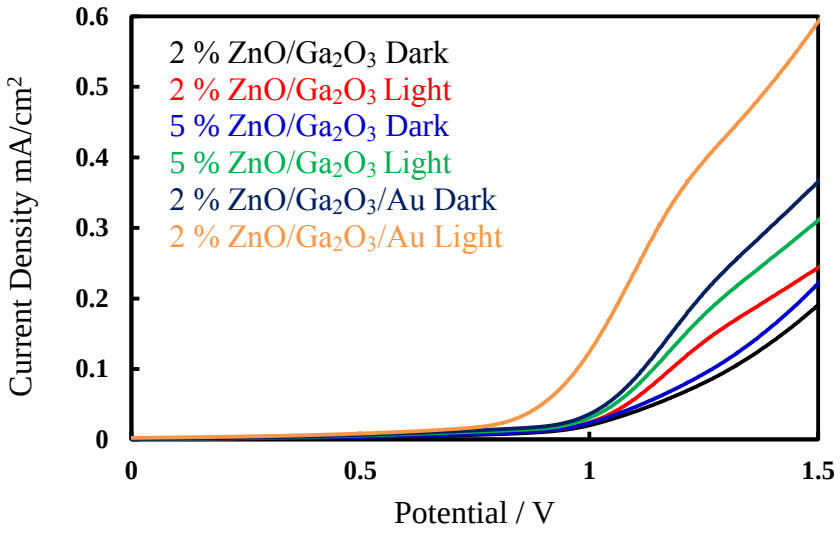

Figure 16: LSVP of 2 %, 5 % ZnO/Ga_2O_3 and 2 % ZnO/Ga_2O_3/Au in the dark and light

CHAPTER 4

Synthesis and Fabrication of Tungsten Oxide/Bismuth Vanadate Photoanode

4.1 Experimental Work

4.1.1 Fabrication of Tungsten Oxide Seeds:

Tungsten oxide seeds was fabricated by physical approach using automatic sputter coater on indium oxide tin oxide coated glass substrate (ITO). Using WO_3 target, Base pressure was 9.1 x 10^{-6} Pa and working pressure was 2 x 10^{-3} Pa, the duration of deposition was 2 min using 80 W power.

4.1.2 Synthesis of Tungsten Oxide/Bismuth Vanadate Hetero-structure:

Hetero-structured of $WO_3/BiVO_4$ nanoarrays was synthesized by hydrothermal approach as in literature [33, 34]. Bismuth vanadium oxide ($BiVO_4$) precursor solution was prepared by mixing (0.137 M) from vanadium (V) oxide V_2O_5 (99.99%, Sigma Aldrich) and (0.052 M) bismuth (III) nitrate pentahydrate Bi $(NO_3)_3.5H_2O$ (99.99%, Sigma Aldrich) in 200 ml nitric acid (2 M) HNO_3.

Hetero-structure of ($WO_3/BiVO_4$) was synthesized by adding tungsten oxide (0.050 M) solution previously prepared to the $BiVO_4$ precursor solution. Then the mixture of $WO_3/BiVO_4$ solution was transferred into a Teflon vessel, sealed in an autoclave and maintained in an oven at 120 °C for 24 hours. The product was removed, dried and calcined at high temperature 500 °C for 3 hours. The synthesis process are showing in the

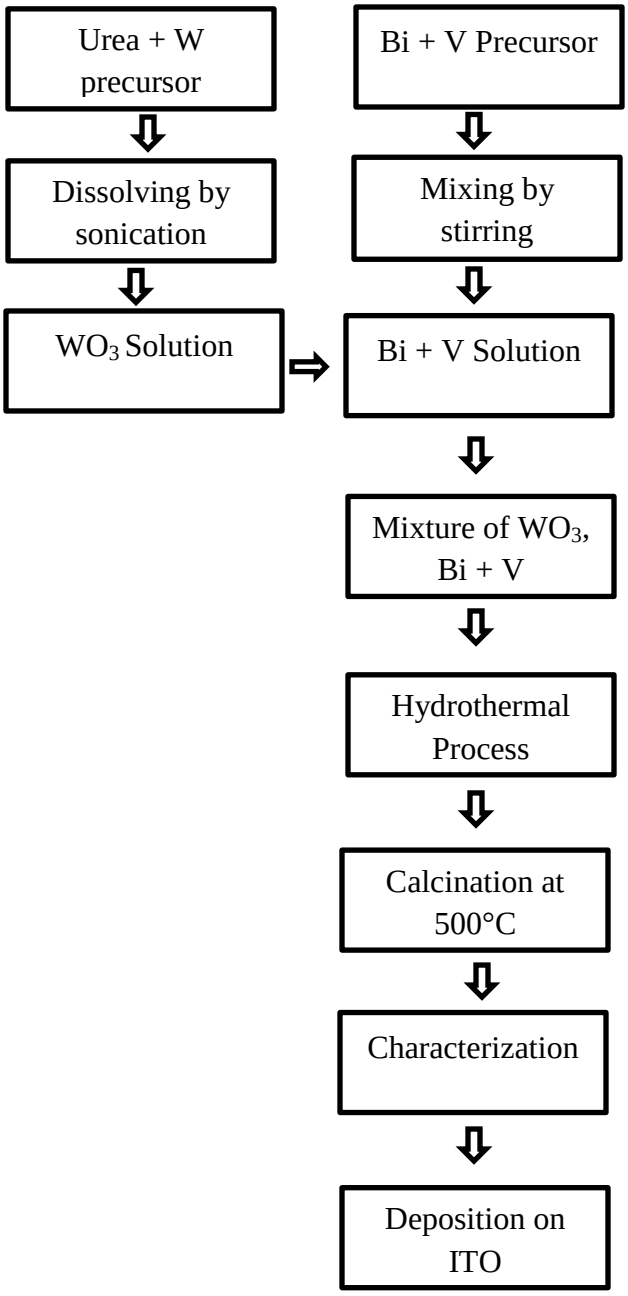

Figure 17: Schematic representation of the fabrication of $WO_3/BiVO_4$ thin film

scheme above see figure (17).

4.1.3 Characterization:

4.1.3.1 XRD and Raman Spectroscopy:

The crystalline structure of the hetero-structures were analyzed by powder X – Ray Diffractometer rigaku rint – 2500. Radiation: Cu Ka lamb: 1.54060, $\lambda = 1.54056$ A, in the range of 10 – 60 in 2 θ degree, scan rate was 3 sec. Powder samples and thin film were placed on the glass plate.

The Raman analysis were performed at room temperature using Yvon Jobin Horiba Raman spectrometer (iHR 320) model with CCD detector. The laser source was green type at 532 nm line and intensity was 45 %. The spectrums were obtained from the scattered light normal to the sample surface, with grating position 600 mm, slit width 96 cm, accumulation number 3 and exposure time 10 sec.

4.1.3.2 FESEM, EDS Analysis:

The surface morphology of these materials were analyzed by field emission scanning electron microscope (FESEM). The compositional analysis was carried out by EDS equipped with FESEM instrument. Powder samples and thin film were mounted on the sample holder using double sided copper conductive tape.

4.1.3.3 Optical Measurements:

Room temperature photoluminescence was carried out using Yvon Jobin Horiba instrument model no FL3- 2iHR. UV – VIS analysis was investigated at room temperature by Cary series UV – VIS – NIR spectrometer.

4.1.3.4 Photoelectrochemical (PEC) Set-up:

The photoelectrochemical measurements were investigated according to the standard photoelectrochemical work station [152]. Chronoamperometry (CA) and linear sweep voltammetry potentiostatic (LSVP) were conducted using three electrode set-up, calomel (Hg / Hg_2CL_2) and platinum as reference and counter electrode respectively in 0.5 M

Na_2SO_4 [PH = ~7] electrolyte. Metrohm autolab (B.V) Potentiostat / Galvanostat PGSTAT 10 was used to investigate the photocurrent at a scan rate of 0.0999 V/s, coupled with oriel sol 3A class AAA solar simulator 100 mW/cm^2 and 1.5 AM (1 sun, Oriel) as a source of illumination. All photoelectrochemical analysis are explaining here according to the normal hydrogen electrode (NHE).

4.2 Results and Discussion:

4.2.1 Formation of Tungsten Oxide Seeds:

Tungsten oxide seeds were deposited on the ITO substrate using automatic sputter coater as physical approach as in Figure (18 a) which is illustrating powder XRD of bare ITO and WO_3 seeds it is clear that the entire substrate has been covered by WO_3 seeds because all the ITO diffraction peaks 29.62, 30.19, 37.59, 40.49, 44.47, 48.31, 48.95 which are corresponding to growth direction (003), (12-1), (220), (104), (303), (042) and (23-1) with (JCPDS #: 01-077-8214) have been disappeared, and (002), (020), (200), (120), (121), (022), (-202) and (202) belong to monoclinic WO_3 with (JCPDS #: 00-043-1035) appear at 23.12, 23.59, 24.38, 26.59, 29.14, 33.27, 33.57 and 34.15 respectively.

The morphology of seeds layer have been investigated by FESEM and revealed the homogeneity of the seeds on the entire substrate with smooth and uniform surface. In addition to the surface the size of the WO_3 seeds was extremely small. Thus, it is difficult to discriminate between bare ITO and WO_3 seeds by naked eye as in Figure (18 b & c). Furthermore the compositional characterization has been carried out by EDS coupled with FESEM and showed the presence of W and O atom as in figure (18 d) along with ITO substrate component.

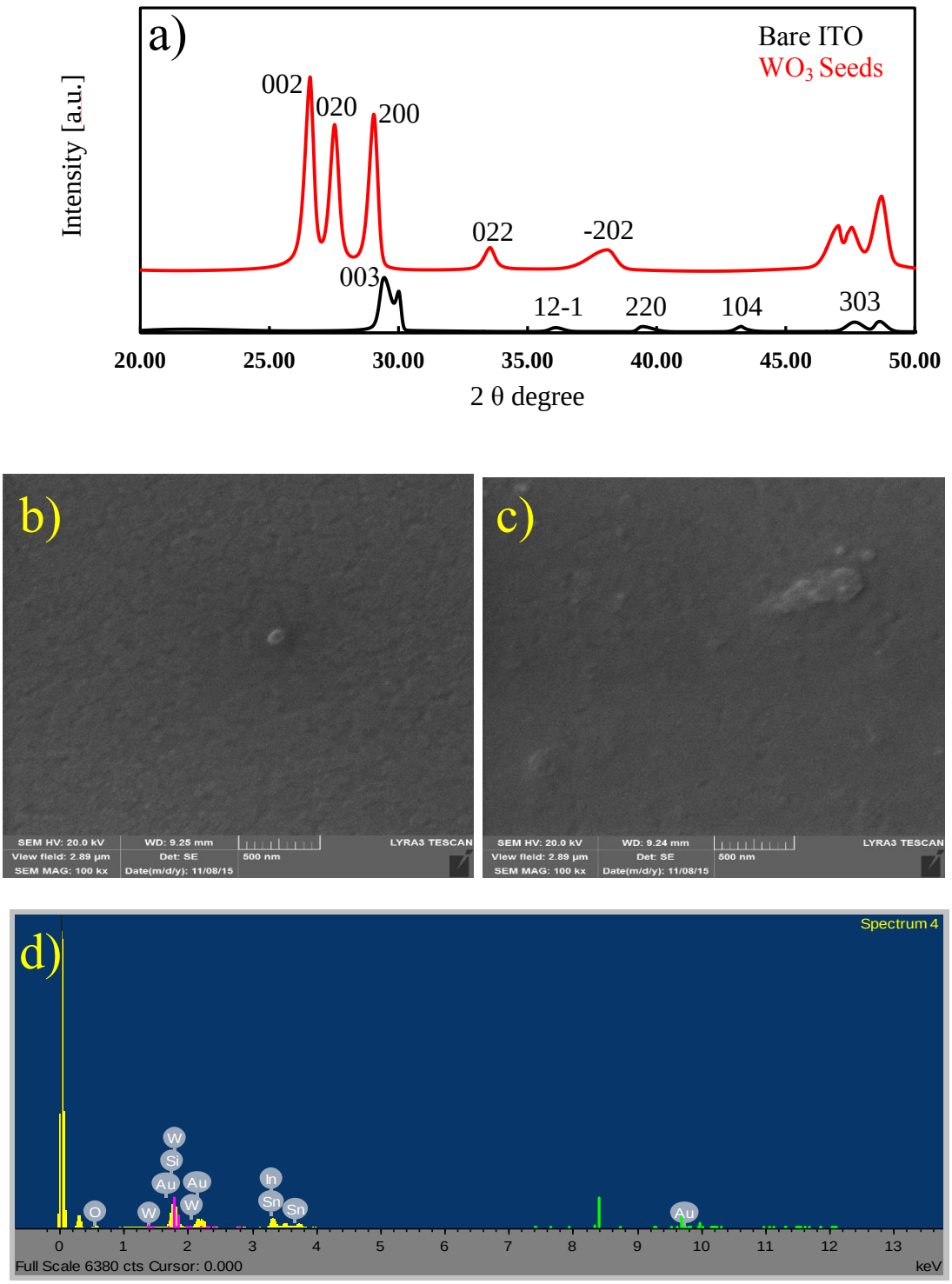

Figure 18: a) XRD of bare ITO, WO_3 Seeds. FESEM of b) bare ITO, c) WO_3 seeds and d) EDS analysis of WO_3 seeds

4.2.2 Fabrication of Tungsten Oxide/Bismuth Vanadate Hetero-structure:

Tungsten oxide/bismuth vanadate hetero-structure were synthesized via hydrothermal approach. XRD was carried out to study the textured properties. From XRD pattern as in Figure (19) $WO_3/BiVO_4$ showed peaks at 28.62, 32.64, 52.33 and 55.06 corresponding to (103), (110), (211) and (213) respectively. The $WO_3/BiVO_4$ has polycrystalline structure with tetragonal phase in crystal system (JCPDS #: 00-047-0478). With residual characteristic peaks of pure WO_3 in the directions of (002), (200), (-202) (023) (004) corresponding to 23.28, 24.52, 34.22, 42.60, and 47.62 in 2 θ degree (JCPDS #: 00-043-1035) and $BiVO_4$ (002), (011) and (004) which are belonging to 15.62, 19.18

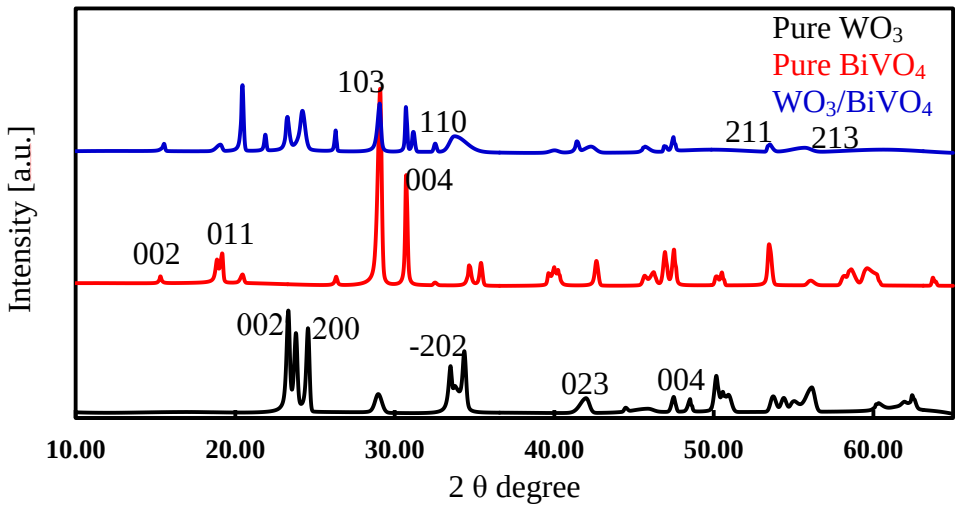

Figure 19: XRD analysis of pure WO_3, pure $BiVO_4$ and $WO_3/BiVO_4$ nanoflakes

and 30.76 in 2 θ degree (JCPDS**#:** 01-083-1699) at 2 θ degree respectively as in figure (19).

For detailed structural elucidation Raman spectra was investigated for pure WO_3, pure $BiVO_4$ and $WO_3/BiVO_4$ individually for the calcined powders. The intensive Raman

peaks at 809 and 720 cm^{-1} associated with stretching W-O-W bond and the bending modes of W-O-W bridging oxide ions at 273 and 329 cm^{-1} in the pure WO_3 [167]. The asymmetric and symmetric deformation modes of the $(VO_4)^{3-}$ tetrahedron recorded peaks at 327 and 367 cm^{-1}. The characteristic Raman peak at 823 cm^{-1} corresponding to the symmetric V-O bond [168] has been shifted and changed in their intensities with the appearance of new peaks for instance at 137, 699.7, 808.8 cm^{-1} respectively, these shift and change might be attributed to the formation of hetero-structure see Figure (20). The enlarged figure of $WO_3/BiVO_4$ hetero-structure illustrated in Figure (34 b) appendix (B).

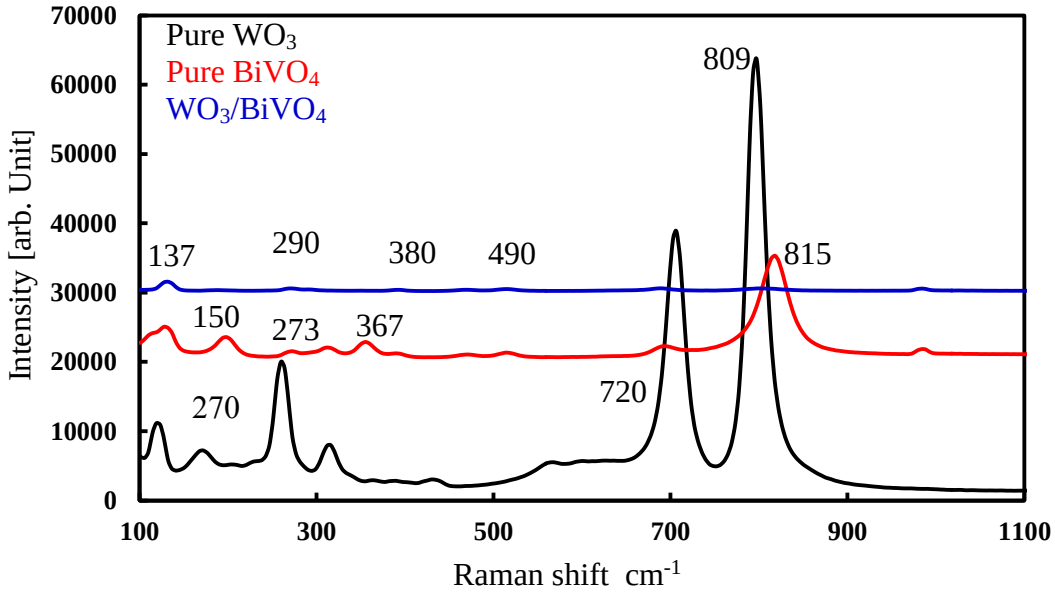

Figure 20: Raman spectrum of WO_3, $BiVO_4$ and $WO_3/BiVO_4$ nanoflakes

The morphology of the synthesized hetero-structure has been viewed using FESEM at low and high magnification. Figure (21 a & b), illustrate the formation of $WO_3/BiVO_4$ thin film nanoflakes like morphology due to an assembly of intertwined platelets radiating in whole directions [44]. The surface was smooth and no grain was observed. The compositional analysis (EDS) of $WO_3/BiVO_4$ hetero-structure has been investigated

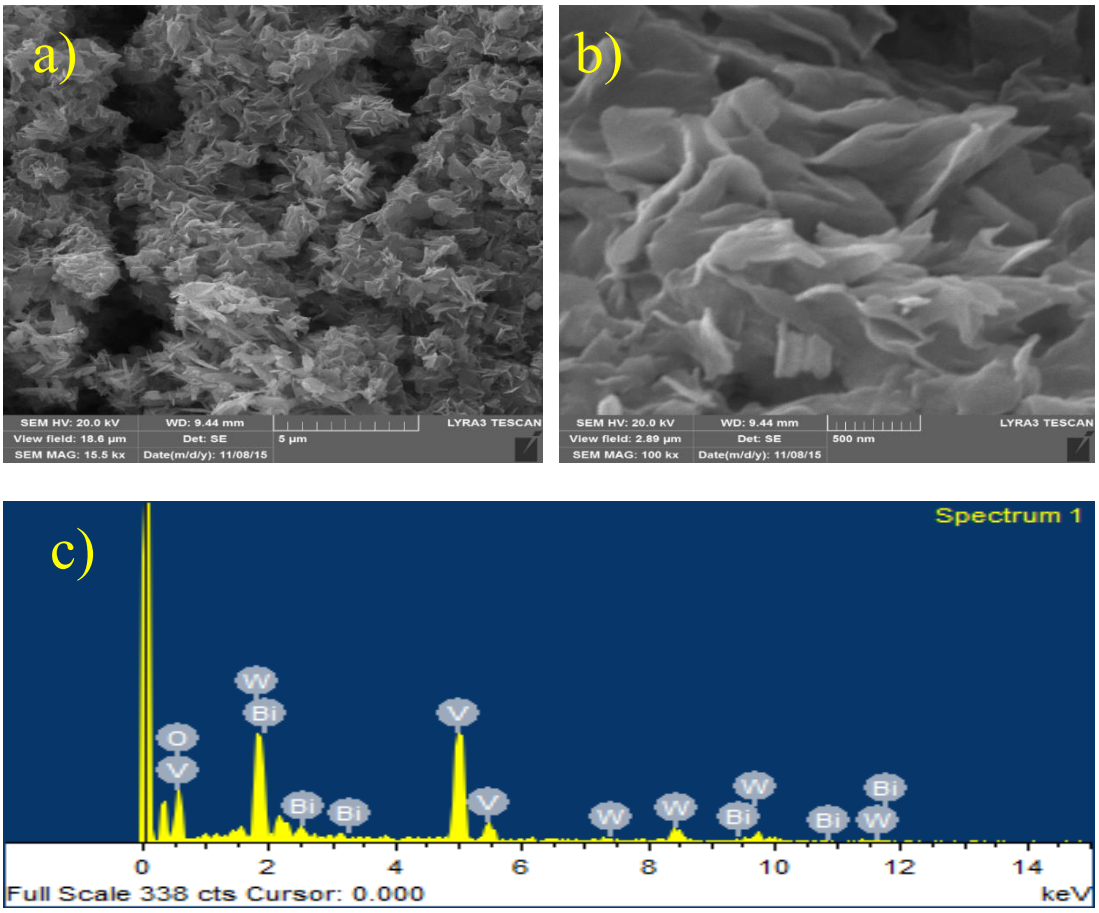

Figure 21: FESEM of $WO_3/BiVO_4$ nanoflakes at a) low magnification b) high magnification and c) EDS analysis of $WO_3/BiVO_4$ nanoflakes

as in Figure (21 c) and confirmed the presence of W, Bi, V, and O. The atomic ratio of W and V was close to the stoichiometric ratio.

The optical properties of the $WO_3/BiVO_4$ nanoflakes hetero-structure have been revealed using UV – VIS – NIR spectrometer. UV – VIS absorption of these metal oxides have been depicted. Small absorption onset have been observed at 496 nm for WO_3, while the onset of absorption of $BiVO_4$ was at 579 nm which is shifted toward visible region. As a result, of addition of WO_3 to $BiVO_4$ nanostructure slight shift have been recorded for $WO_3/BiVO_4$ hetero-structure in absorption and it was at 583 nm as in Figure

(22 a). Furthermore, the diffuse reflectance spectra has been carried out as a direct relation of Kubelka-Munk function F(R) with photon energy *h*v (eV) in the range (0 – 5 eV) by the same machine for band gap estimation. $F(R) = (1 - R)^2/2R$ is the relation give Kubelka – Munk function, where R is the magnitude of reflectance [159]. The band gaps were determinate by extrapolating the linear part of $F(R)^2$ curve (y axis) until intersects with (x axis) which is the energy (eV). Generally, in the reflectance spectra low values of reflectance mean high absorption in the specific location of wavelength. The tungsten oxide film reported band gap around 2.7 eV illustrate good transparency in visible region. The band gap of $BiVO_4$ thin film was 2.37 eV. As a result of fabrication of hybrid $WO_3/BiVO_4$ semiconductor, the band gap has been shifted slightly to be 2.24 eV as in Figure (22 b). This is indicates that $WO_3/BiVO_4$ photoanode can harvest visible light in solar energy efficiently [162]. This variation in band gap can be attributed to changing in the crystal structure due to adding WO_3 to $BiVO_4$ as earlier we noticed from XRD analysis. The changing in optical properties of semiconductors has been investigated generally by many researchers, illustrated that the optical band gap can be vary as a result of different reasons such as the particle sizes. Particularly, Zheng et al. [165] studied the effect of annealing temperature in the ZnO nanoparticles, they reported that with the increasing the annealing temperature the band – edge absorption begins at larger wavelength. They also noticed that the red shift in optical gap with more particle size it can be due to change in morphology. With respect to annealing temperature they suggested that the beginning of band-edge absorption at larger wavelength is due to high annealing temperature which formed defects in the samples. These results are consistent with UV – VIS absorption results.

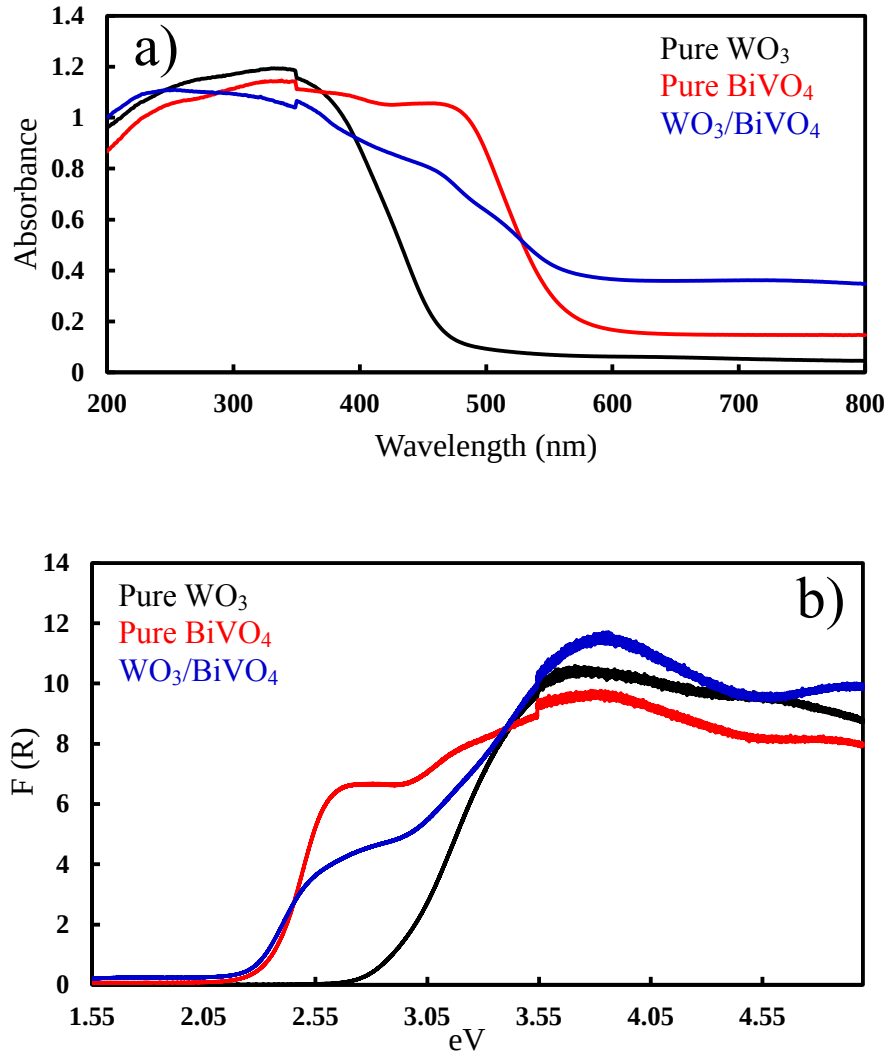

Figure 22: a) UV - VIS and b) reflectance spectrums of pure WO_3, pure $BiVO_4$ and $WO_3/BiVO_4$ nanoflakes

Table 3: UV – VIS onsets and band gap energies of WO_3, $BiVO_4$ and $WO_3/BiVO_4$

Structure	UV – VIS Onset (nm)	Band gap (eV)
WO_3	460	2.7
$BiVO_4$	540	2.3
$WO_3/BiVO_4$	554	2.24

4.2.3 Photoelectrochemical Properties:

The photoelectrochemical measurements of the $WO_3/BiVO_4$ photoanode were investigated in three electrode set-up. Calomel, platinum and $WO_3/BiVO_4$ thin film as reference, counter electrode and Working photoelectrode respectively in 0.5 M Na_2SO_4 (PH = ~7) electrolyte. Metrohm autolab (B.V) Potentiostat / Galvanostat PGSTAT 10 used as a potential source. Solar simulator class 3A (Oriel) was used as illumination source, the photoanode was exposed to the front side illumination (through ITO) with 1.5 AM (1 sun) simulated solar class 3A (Oriel). Chronoamperometry measurements (J p) versus time (t) profiles was conducted to verify the stability of the semiconductor. At neutral pH $WO_3/BiVO_4$ photoanode was steady and no significant degradation was noticed during the illumination [162]. We noticed a similar J p – t profile that depend on J p spike after first irradiation, which is relaxed to stable plateau exploring the significant stability of the semiconductor [165] as in Figure (23).

Then linear sweep voltammetry potentistatic (LSVP) was carried out for further investigation of photoelectrochemical properties with previous set-up from 0 to 0.5 V versus normal hydrogen electrode (NHE). $WO_3/BiVO_4$ has been deposited on the ITO (0.5 cm X 0.85 cm) substrate by normal drop – casting and annealed at different temperatures 200 °C and 450 °C, respectively, to study the effect of annealing temperatures and light for $WO_3/BiVO_4$ thin film. These photoanodes were active toward oxygen evolution reaction (OER). The photocatalytic activities of $WO_3/BiVO_4$ photoanode were enhanced significantly with increasing annealing temperatures and reached it maximum which were 0.078 and 0.080 mA/cm^2 for 200 °C and 450 °C respectively at 0.33 V in the absence of light see Figure (24). To study the effect of light

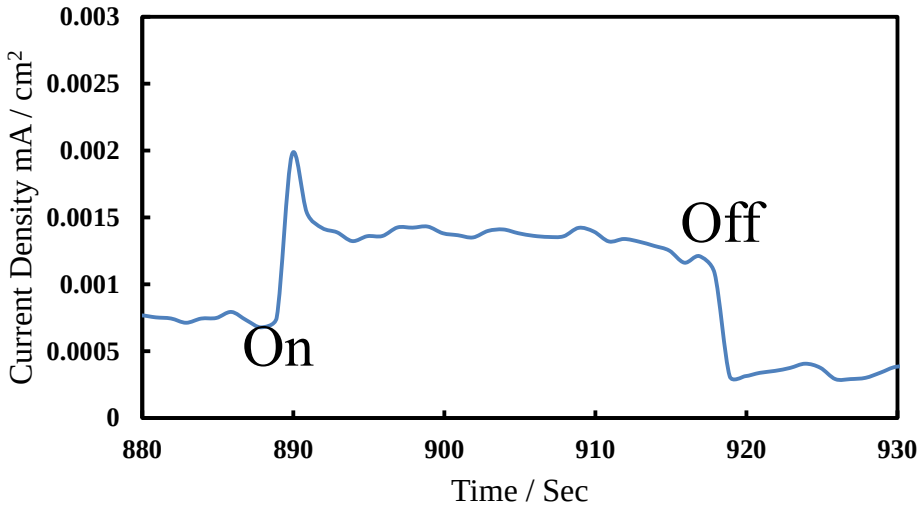

Figure 23: Chronoamperometry of $WO_3/BiVO_4$ photoanode with on/off mode

for both annealing temperature, both photoanodes annealed at 200 °C and 450 °C have been exposed to the visible light irradiation. Thus the activities of both photoanodes were improved slightly compared to the dark. The current density achieved were 0.106 and 0.109 mA/cm^2 for 200 °C and 450 °C at 0.5 V see Figure (24). The photoelectrochemical behavior enhanced with increasing the annealing temperatures and this can be attributed to the excellent charge separation and improved crystallites of the $WO_3/BiVO_4$ nanoflakes annealed at 450 °C. The effect of light has been investigated for the similar annealing temperature, for example annealed at 200 °C, the achieved photocurrent were (0.106 mA/cm^2) in the light compared to the dark (0.082 mA/cm^2) at 0.5 V see Figure (35 a) in appendix B, and this can be refer to the light impact on the photoanode. The aggregation of the crystal has a crucial impact on recombination rate of photogenerated electrons and this is direct proportion to the grain size of the crystal, the grain size of the metal oxides can enhanced with increasing annealing temperature due to the steady gene-

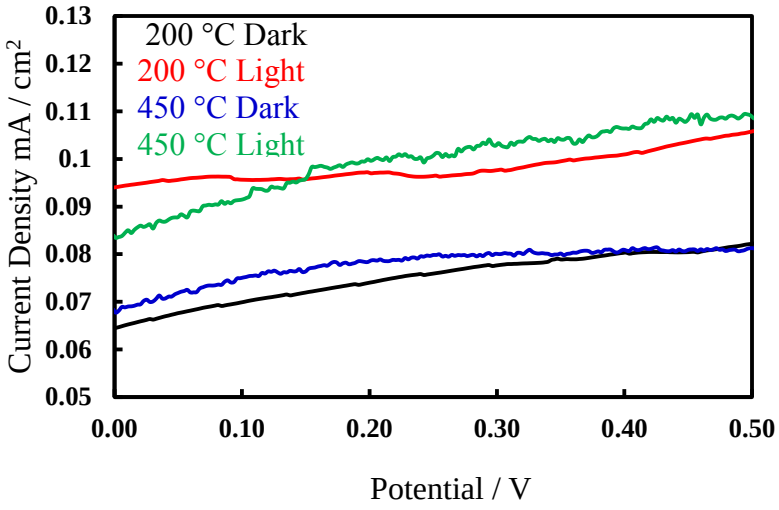

Figure 24: LSVP of $WO_3/BiVO_4$ nanoflakes annealed at 200 °C and 450 °C in the dark and light

ration of bluk crystalliets of metal oxides at higher temperature. The life-time and quantity of photo-generated electrons are other crucial parameters in photoelectrochemical measurement. Photo-generated electrons in the crystallites are transported to the $WO_3/BiVO_4$ surface and aggregated on pt electrode, thus the photoelectrochemical process could accelerated on it. Therefore the photoelectrochemical activity in the $WO_3/BiVO_4$/Pt system affected by the recombination rate of the photo-generated electrons in the $WO_3/BiVO_4$ crystallites. The large size of the crystals, are travelling long distances and this lead to quick recombination opportunity of photo-generated electrons, and enhance the oxygen vacancy related defect, as well as it can consume the photo-generated electrons if annealed at higher temperature beyond 950 °C as Gang Xin et al reported [166]. The enhanced photocurrent of the $WO_3/BiVO_4$ photoanode has been obtained by combing the advantage of the light harvesting of $BiVO_4$ and the efficiency of light conversion of WO_3 [167]. As electron transported from $BiVO_4$

to WO_3 charge separation was enhanced dramatically. The valence and conduction band of WO_3 is more positive in energy than those of $BiVO_4$, which is facilitate such charge separation. Photo-generated holes from excited WO_3 are transported into valence band of $BiVO_4$, this in turn enhancing the charge separation of the $WO_3/BiVO_4$ hybrid semiconductor. Typically the recombination rate of h^+ - e^- couples within $BiVO_4$ decreased.

Chapter 5

Conclusions and Recommendations

In this thesis work we report the essential synthesis, fabrication, characterization and practical results of two (2) hybrid metal oxide nanoarrays ZnO/Ga_2O_3 and $WO_3/BiVO_4$ thin films. The impact of various parameters are highlighted in the discussion. The texture, structural, optical and morphological properties of these photoanodes are investigated. The potential utilization of these metal oxides were attempted and demonstrated for future studies.

5.1 Fabrication of ZnO/Ga_2O_3 thin film:

ZnO/Ga_2O_3 thin films were successfully synthesized and fabricated on ITO substrate in two steps via physical approach and hydrothermal method, from aqueous solution containing 0.03 M of ZnO and various amount of Ga_2O_3 at low temperature. The XRD analysis revealed that the synthesized materials have polycrystalline structure with orthorhombic system, High magnification FESEM illustrated well aligned nanorods on ITO substrate with hexagonal shape on the surface of the rods. The photoresponse of ZnO/Ga_2O_3 photoanode represented the activity toward oxygen evolution reaction for the photoanode. Chronoamperometry and linear sweep voltammetry potentiostatic showed the stability of the thin film versus photo-corrosion and the photocurrent increased gradually with increasing Ga_2O_3 amounts and dramatically by Gold (Au) coating regarding-less to Ga_2O_3 amounts. As future work and recommendations for ZnO/Ga_2O_3

thin film we recommend to perform nitradation or oxynitradation with complete investigation of photocatalytic activity.

5.2 Fabrication of $WO_3/BiVO_4$ thin film:

Hetero-structure of $WO_3/BiVO_4$ nanoarrays were successfully synthesized and fabricated on ITO substrate in two steps via physical approach and hydrothermal method, from aqueous solution containing (0.137 M) of $BiVO_4$ and (0.050 M) of WO_3. The XRD analysis revealed that the synthesized materials have polycrystalline structure with tetragonal crystal system, low and high magnification FESEM illustrated flakes like shape have been fabricated on the entire ITO substrate. The photoresponse of $WO_3/BiVO_4$ photoanode represented the activity toward oxygen evolution reaction for the photoanode. Chronoamperometry and linear sweep voltammetry potentiostatic showed the stability of the thin film versus photo-corrosion and the photocurrent increased with the increasing of annealing temperature. As future work and recommendations for $WO_3/BiVO_4$ thin film we recommend to explore nitridation or oxynitridation with complete investigation of photocatalytic activity.

References:

[1] Murray, J. & King, D. Climate policy: Oil's tipping point has passed, *Nature* 481, 433-435 2012.

[2] The Energy Report: 100% Renewable Energy by 2050, 2011.

[3] http://co2now.org/ accessed February 2013.

[4] IPCC Fourth Assessment Report: Climate Change 2007, Working Group I Report: "The Physical Science Basis", 2007.

[5] European Commission, A Roadmap for moving to a low carbon economy in 2050, 2011.

[6] Faunce, T. A.; et al. Energy Environ. Sci 6, 695, 2013

[7] Lewis, N. S.; Nocera, D. G. Proc. Natl. Acad. Sci. 103, 15729, 2006

[8] Barber, J. Chem. Soc. Rev. 2009, 38, 185. Faunce, T.; et al. Energy Environ. Sci. 6, 1074, 2013

[9] R. E. R. Bjorn Marsen , Eric L. Miller , D. Paluselli , Int. J. Hydrogen Energy 32, 3110 – 3115, 2007

[10] M. K. S. Vidhya Chakrapani , J. Thangala , *Int. J. Hydrogen Energy 34* , 9050-9059 , 2009

[11] J. Su , L. Guo , N. Bao , C. Grimes , *Nano Lett. 11*, 1928 – 1933, 2011

[12] H. Kim , J. Kim , W. Kim , W. Choi , *J. Phys. Chem. C , 115* ,-9805, 2011

[13] Benck, J. D.; Hellstern, T. R.; Kibsgaard, J.; Chakthranont, P.; Jaramillo, T. F. *ACS Catal. 4*, 3957–3971, 2014

[14] Laursen, A. B.; Kegnæs, S.; Dahl, S.; Chorkendorff, I. *Energy Environ. Sci.5*, 5577 , 2012

[15] Y. Lin, G. Yuan, R. Liu, S. Zhou, S. W. Sheehan and D. Wang, *Chem. Phys. Lett.*, 507, 209-215, 2011

[16] Segets, D.; Gradl, J.; Taylor, R.K.; Vassilev, V.; Peukert, W. Analysis of optical absorbance spectra for the determination of ZnO nanoparticle size distribution, solubility, and surface energy. *ACS Nano 3*, 1703–1710, 2009

[17] Lou, X. Development of ZnO series ceramic semiconductor gas sensors. *J. Sens. Trans. Technol. 3*, 1–*5*, 1991

[18] K. Fujishima , A. Honda , *Nature. 238* , 37 – 38, 1972

[19] Gratzel, M. Nature. 414, 338, 1991

[20] Y. Park , K. J. McDonald , K.-S. Choi , *Chem. Soc. Rev. 42* , 2321 – 37, 2013

[21] Dulub O, Boatner L A and Diebold U 2002 *Surf. Sci.* 519**,** 201.

[22] Meyer B and Marx D 2003 *Phys. Rev.* B 67 035403

[23] Tasker P W *J. Phys. C: Solid State Phys.* 12 4977, 1979

[24] Dulub O, Diebold U and Kresse G *Phys. Rev. Lett.* 90, 016102, 2003

[25] Wander A, Schedin F, Steadman P, Norris A,McGrath R, Turner T S, Thornton G and Harrison NM *Phys. Rev. Lett.* 86 3811, 2001

[26] Staemmler V, Fink K, Meyer B, Marx D, Kunat M, Gil Girol S, Burghaus U and Woll Ch *Phys. Rev. Lett.* 90**,** 106102, 2003

[27] K. Ikarashi, J. Sato, H. Kobayashi, N. Saito, H. Nishiyama, Y. Inoue, J. Phys. Chem. B 106, 35, 9048–9053, 2002

[28] K. Maeda, T. Takata, M. Hara, N. Saito, Y. Inoue, H. Kobayashi, K. Domen, J. Am. Chem. Soc. 127, 23, 8286–8287, 2005

[29] K. Maeda, K. Teramura, T. Takata, M. Hara, N. Saito, K. Toda, Y. Inoue, H. Kobayashi, K. Domen, J. Phys. Chem. B 109, 43, 20504–20510, 2005

[30] K. Maeda, K. Teramura, K. Domen, Catal. Surv. Asia 11, 4, 145–157, 2007

[31] K. Maeda, K. Teramura, D. Lu, T. Takata, N. Saito, Y. Inoue, K. Domen, Nature 4 40, 7082, 294–295, 2006

[32] K. Maeda, K. Teramura, N. Saito, Y. Inoue, K. Domen, Bull. Chem. Soc. Jpn. 80, 5 1004–1010, 2007

[33] T.G. Deutsch, C.A. Koval, J.A. Turner, J. Phys. Chem. B 110, 50, 25297– 25307 , 2006

[34] H. Wang, J.A. Turner, ECS Trans. 2, 27, 125–133, 2007

[35] J. A. Kohn, G. Katz, and J. D. Broder: Am. Mineral. 42, 398, 1957

[36] S. Geller: J. Chem. Phys. 33**,** 676, 1960

[37] L. Pauling: *Nature of the Chemical Bond* (Cornell University Press, Ithaca, New York) 3rd ed. Chap. 13, Sec. 6, 1960

[38] L. M. Foster and H. C. Stumpf: J. Am. Chem. Soc. 73, 1590, 1951

[39] M. Ogita, K. Higo, Y. Nakanishi, and Y. Hatanaka: Appl. Surf. Sci. 175-176, 721 , 2011

[40] M. Orita, H. Ohta, M. Hirano, and H. Hosono: Appl. Phys. Lett. **77,** 25, 4166 , 2000

[41] R. Jalilian, M. M. Yazdanpanah, B. K. Pradhan, and G. U. Sumanasekera: Chem. Phys. Lett. 426, 393, 2006

[42] M. Fleischer and H. Meixner: Sens. Actuators B 4, 437, 1991

[43] S. Nakagomi, M. Kaneko, and Y. Kokubun: Sens. Lett. 9, 1, 35, 2011

[44] S. Nakagomi, M. Ikeda, and Y. Kokubun: Sens. Lett. 9, 2, 616, 2011

[45] Wrighton, M. S.; Ellis, A. B.; Wolczanski, P. T.; Morse, D. L.; Abrahamson, H. B.; Ginley, D. S. J. Am. Chem. Soc. 98, 10, 2774, 1976

[46] Takata, T.; Tanaka, A.; Hara, M.; Kondo, J. N.; Domen, K. Catal. Today. 44, 1 - 4 , 17, 1998

[47] Osterloh, F. E. Chem. Mater. 20, 35, 2008

[48] Hara, M.; Hitoki, G.; Takata, T.; Konda, J. N.; Kobayashi, H.; Domen, K. Catal. Today. 78, 555, 2003.

[49] Kasahara, A.; Nukumizu, K.; Hitoki, G.; Takata, T.; Kondo, J. N.; Hara, M.; Kobayashi, H.; Domen, K. J. Phys. Chem. A. 106, 6750, 2002

[50] Kasahara, A.; Nukumizu, K.; Takata, T.; Kondo, J. N.; Hara, M.; Kobayashi, H.; Domen, K. J. Phys. Chem. B. 107, 791, 2003

[51] Maeda, K.; Domen, K. Chem. Mater. Rev. 22, 612, 2010

[52] Kudo, A.; Miseki, Y. Chem. Soc. Rev. 38, 253, 2009

[53] Domen, K.; Maeda, K. Mater. Res. Bull. 36, 25, 2011

[54] Jensen, L. L.; Muckerman, J. T.; Newton, M. D. J. Phys. Chem. C. 112, 3439, 2008

[55] Wang, S.; Wang, L. Phys. Rev. Lett. 104, 065501, 2010

[56] Li, L.; Muckerman; James, T.; Hybertsen; Mark, S.; Allen; Philip, B. Phys. Rev. B 83, 134202-1−134202-6, 2011

[57] G. Hodes, D. Cahen, J. Manassen, Nature 260, 5549, 312–313, 1976

[58] K. Sayama, R. Yoshida, H. Kusama, K. Okabe, Y. Abe, H. Arakawa, Chem. Phys. Lett. 277, 4, 387–391, 1997

[59] J.E. Yourey, B.M. Bartlett, J. Mater. Chem. 21, 21, 7651–7660, 2011

[60] N. Naseri, S. Yousefzadeh, E. Daryaei, A.Z. Moshfegh, Int. J. Hydrogen Energy 36 , 21, 13461–13472, 2011

[61] J. Su, X. Feng, J.D. Sloppy, L. Guo, C.A. Grimes, Nano Lett. 11, 1, 203–208, 2010

[62] D. Paluselli, B. Marsen, E.L. Miller, R.E. Rocheleau, Electrochem. Solid-State lett. 8, 11, G301–G303, 2005

[63] B. Cole, B. Marsen, E. Miller, Y. Yan, B. To, K. Jones, M. Al-Jassim, J. Phys. Chem. C 112, 13, 5213–5220, 2008

[64] Y. Sun, C.J. Murphy, K.R. Reyes-Gil, E.A. Reyes-Garcia, J.M. Thornton, N.A. Morris, D. Raftery, Int. J. Hydrogen Energy 34, 20, 8476–8484, 2009

[65] C. Le, S. Shet, T. Houwen, A. Kwang-soon, W. Heli, Y. Yanfa, J. Turner, M. Al-Jassim, J. Appl. Phys. 108, 4, 043502–135024, 2010

[66] Bange, K. Sol. Energy Mater. Sol. Cells. 58, 1−131, 1999

[67] Granqvist, C. G. Sol. Energy Mater. Sol. Cells. 60, 201−262, 2000

[68] Deb, S. K. Sol. Energy Mater. Sol. Cells. 92, 245−258, 2008

[69] Hodes, G.; Cahen, D.; Manassen, J. Nature. 260, 312−313, 1976

[70] Santato, C.; Ulmann, M.; Augustynski, J. J. Phys. Chem. B. 105, 936−940, 2001

[71] Deb, S. K. Appl. Opt. 3, 192−195, 1969

[72] Deb, S. K. Philos. Mag. 27, 801−822, 1973

[73] Berek, J. M; Sienko, M. J. J. Solid State Chem. 2, 109−133, 1970

[74] Butler, M. A.; Nasby, R. D.; Quinn, R. K. Solid State Commun. 19, 1011−1014,

1976
[75] Scaife, D. E. Solar Energy. 25, 41−54, 1980

[76] Tanner, R. E.; Altman, E. I. J. Vac. Sci. Technol. A. 19, 1502−1509, 2001

[77] Chatten, R.; Chadwick, A. V.; Rougier, A.; Lindan, P. J. D. J. Phys. Chem. B. 109 , 3146−3156, 2005

[78] Roussel, P.; Labbe, Rh.; Lelingly, H.; Goult, D.; Foury- Leylekian, P.; Pouget, J. P. Phys. Rev. B. 62, 176−188, 2000

[79] Yakovkin, I. N.; Gutowski, M. Surf. Sci. 601, 1481−1488, 2007

[80] Jones, F. H.; Rawlings, K.; Foord, J. S.; Cox, P. A.; Egdell, R. G.; Pethica, J. B.; Wanklyn, B. M. R. Phys. Rev. B. 52, R14392− R14395, 1995

[81] Jones, F. H.; Dixon, R. A.; Brown, A. Surf. Sci. 369, 343− 350, 1996

[82] Jones, F. H.; Rawlings, K.; Foord, J. S.; Egdell, R. G.; Pethica, J. B.; Wanklyn, B. M. R.; Parker, S. C.; Oliver, P. M. Surf. Sci. 359, 107−121, 1996

[83] Dixon, R. A.; Williams, J. J.; Morris, D.; Rebane, J.; Jones, F. H.; Egdell, R. G.; Downes, S. W. Surf. Sci. 399, 199−211, 1998

[84] Bringans, R. D.; Hochst, H.; Shanks, H. R. Vacuum. 31, 473−475, 1981

[85] Murphy, S.; Mannai, G.; Shvets, I. V. Surf. Sci. 579, 65− 72, 2005

[86] Li, M.; Altman, E. I.; Posadas, A.; Ahn, C. H. Surf. Sci. 542, 22−32, 2003

[87] Li, M.; Altman, E. I.; Posadas, A.; Ahn, C. H. Thin Solid Films. 446, 238- 247 , 2004

[88] Li, M.; Posadas, A.; Ahn, C. H.; Altman, E. I. Surf. Sci. 579, 175−187, 2005

[89] Li, M.; Gao, W; Posadas, A.; Ahn, C. H.; Altman, E. I. J. Phys. Chem. B. 108, 15259−15265, 2004

[90] Ueda, R.; Ichinokawa, T. Phys. Rev. 80, 1106, 1950

[91] Loopstra, B. O.; Rietveld, H. M. Acta Crystallogr. Sect. B: Struct. Crystallogr. Cryst. Chem. B25, 1420−1421, 1969

[92] Diehl, R.; Brandt, G.; Salje, E. Acta Crystallogr. B. 34, 1105−1111, 1978

[93] Kehl, W. L.; Hay, R. G.; Wahl, D. J. Appl. Phys. 23, 212−215, 1952

[94] Matthias, B. T.; Wood, E. A. Phys. Rev. 84, 1255, 1951

[95] Oliver, P. M.; Parker, S. C.; Egdell, R. G.; Jones, F. H. J. Chem. Soc. Faraday Trans. 92, 2049−2056, 1996

[96] Valdés, Á; Kroes, G.-J. J. Chem. Phys. 130, 114701, 2009

[97] Kudo, A.; Omori, K.; Kato, H. A Novel Aqueous Process for Preparation of Crystal Form-Controlled and Highly Crystalline $BiVO_4$ Powder From Layered Vanadates at Room Temperature and Its Photocatalytic and Photophysical Properties. J. Am. Chem. Soc. 121, 11459–11467, 1999

[98] Sayama, K.; Nomura, A.; Zou, Z.; Abe, R.; Abe, Y.; Arakawa, H. photoelectrochemical Decomposition of Water on Nanocrystalline BiVO4 Film Electrodes Under Visible Light. Chem. Commun. 2003, 2908–2909.

[99] Su, J.; Guo, L.; Yoriya, S.; Grimes, C. A. Aqueous Growth of Pyramidal-Shaped $BiVO_4$ Nanowire Arrays and Structural Characterization: Application to photoelectrochemical Water Splitting. Cryst. Growth Des. 2010, 10, 856–861.

[100] Iwase, A.; Kudo, A. Photoelectrochemical Water Splitting Using Visible-Light-Responsive $BiVO_4$ Fine Particles Prepared in an Aqueous Acetic Acid Solution. J. Mater. Chem. DOI:10.1039/c0jm00961j, 2010

[101] Long, M.; Cai, W.; Kisch, H. Visible Light Induced Photoelectrochemical properties of n-$BiVO_4$ and n-$BiVO_4$/p-Co_3O_4. J. Phys. Chem. C. 112, 548–554, 2008

[102] Sayama, K.; Nomura, A.; Arai, T.; Sugita, T.; Abe, R.; Yanagida, M.; Oi, T.; Iwasaki, Y.; Abe, Y.; Sugihara, H. Photoelectrochemical Decomposition of Water into H_2 and O_2 on Porous $BiVO_4$ Thin-Film Electrodes under Visible Light and significant Effect of Ag Ion Treatment. J. Phys. Chem. B. 110, 11352–11360, 2006

[103] Park, Y.; McDonald, K. J.; Choi, K. S. Progress in Bismuth Vanadate Photoanodes for Use in Solar Water Oxidation. Chem. Soc. Rev. 42, 2321−2337, 2013

[104] Zhang, L.; Chen, D. R.; Jiao, X. L. Monoclinic Structured $BiVO_4$ Nanosheets: Hydrothermal Preparation, Formation Mechanism, and Coloristic and photocatalytic Properties. J. Phys. Chem. B. 110, 2668−2673, 2006

[105] Zhou, L.; Wang, W. Z.; Zhang, L.; Xu, H. L.; Zhu, W. Singlecrystalline $BiVO_4$ Microtubes with Square Cross-sections: Microstructure, Growth Mechanism, and Photocatalytic Property. J. Phys. Chem. C. 111, 13659−13664, 2007

[106] Abdi, F. F.; Firet, N.; van de Krol, R. Efficient $BiVO_4$ Thin Film Photoanodes Modified with Cobalt Phosphate Catalyst and W-doping. Chem Cat Chem. 5, 490

– 496, 2013

[107] Li, Z. S.; Luo, W. J.; Zhang, M. L.; Feng, J. Y.; Zou, Z. G. Photoelectrochemical Cells for Solar Hydrogen Production: Current State of Promising Photoelectrodes, Methods to Improve Their Properties, and Outlook. Energy Environ. Sci. 6, 347 - 370, 2013

[108] Abdi, F. F.; van de Krol, R. Nature and Light Dependence of Bulk Recombination in Co-Pi-Catalyzed $BiVO_4$ Photoanodes. J. Phys. Chem. C. 116, 9398−9404, 2012

[109] Ding, C. M.; Shi, J. Y.; Wang, D. G.; Wang, Z. J.; Wang, N.; Liu, G. J.; Xiong, F. Q.; Li, C. Visible Light Driven overall Water Splitting Using Cocatalyst/$BiVO_4$ Photoanode with Minimized Bias. Phys. Chem. Chem. Phys. 15, 4589−4595, 2013

[110] Berglund, S. P.; Flaherty, D. W.; Hahn, N. T.; Bard, A. J.; Mullins, C. B. Photoelectrochemical Oxidation of Water Using Nanostructured $BiVO_4$ Films. J. Phys. Chem. C. 115, 3794−3802, 2011

[111] Jia, Q. X.; Iwashina, K.; Kudo, A. Facile Fabrication of An Efficient $BiVO_4$ Thin Film Electrode for Water Splitting under Visible Light Irradiation. Proc. Natl. Acad. Sci.U.S.A. 2012, 109, 11564−11569.

[112] Seabold, J. A.; Choi, K. S. Efficient and Stable Photo-Oxidation of Water by a Bismuth Vanadate Photoanode Coupled with an Iron Oxyhydroxide Oxygen Evolution Catalyst. J. Am. Chem. Soc. 134, 2186−2192, 2012

[113] Liang, Y. Q.; Tsubota, T.; Mooij, L. P. A.; van de Krol, R. Highly Improved Quantum Efficiencies for Thin Film $BiVO_4$ Photoanodes. J. Phys. Chem. C. 115, 17594−17598, 2011

[114] Saito, R.; Miseki, Y.; Sayama, K. Highly Efficient Photoelectrochemical Water Splitting Using a Thin Film Photoanode of $BiVO_4/SnO_2/WO_3$ Multi-composite in A Carbonate Electrolyte. Chem. Commun. 48, 3833−3835, 2012

[115] Chen, L.; Graham, M. E.; Li, G. H.; Gray, K. A. Fabricating Highly Active Mixed Phase TiO_2 Photocatalysts by Reactive DC Magnetron Sputter Deposition. Thin Solid films. 515, 1176− 1181, 2006

[116] Di Franco, F.; Santamaria, M.; Di Quarto, F.; Tsuji, E.; Habazaki, H. The influenc Of Nitrogen Incorporation on the Optical Properties of Anodic Ta_2O_5. electrohim Acta. 59, 382−386, 2012

[117] Marsen, B.; Miller, E. L.; Paluselli, D.; Rocheleau, R. E. Progress in Sputtered tungsten Trioxide for Photoelectrode Applications. Int. J. Hydrogen. Energy. 32, 3110 – 3115, 2007

[118] Berglund, S. P.; Rettie, A. J. E.; Hoang, S.; Mullins, C. B. Incorporation of Mo

and W into Nanostructured $BiVO_4$ Films for Efficient Photoelectrochemical Water oxidation. Phys. Chem. Chem.Phys. 14, 7065−7075, 2012

[119] Bierlein, J. D. & Sleight, A. W. Ferroelasticity in $BiVO_4$, Solid State communications 16, 69 – 70, 1975

[120] Sleight, A. W., Chen, H. Y., Ferretti, A., & Cox, D. E. Crystal-Growth and structure of $BiVO_4$, *Mater. Res. Bull.* 14, 1571-1581, 1979

[121] Zhao, Z. Y., Luo, W. J., Li, Z. S., & Zou, Z. G. Density functional theory study of doping effects in monoclinic clinobisvanite $BiVO_4$, *Physics Letters A* 374, 4919-4927, 2010

[122] Dreyer, G. & Tillmanns, E. Dreyerite -Natural, Tetragonal Bismuth vanadate from Hirschhorn-Pfalz, *Neues Jahrbuch fur Mineralogie- Monatshefte.* 151-154, 1981

[123] Tokunaga, S., Kato, H., & Kudo, A. Selective preparation of monoclinic and tetragonal $BiVO_4$ with scheelite structure and their photocatalytic properties, *Chem. Mate*13, 4624-4628, 2001

[124] Bhattacharya, A. K., Mallick, K. K., & Hartridge, A. Phase transition in $BiVO_4$, Mater, *Lett.* 30, 7-13, 1997

[125] Roth, R. S. & Waring, J. L. Synthesis and Stability of Bismutotantalite, Stibiotantalite and Chemically Similar ABO_4 Compounds, *American Mineralogist* 48, 1348, 1963

[126] Tilley, S. D., Cornuz, M., Sivula, K., & Grätzel, M. Light-Induced Water splitting With Hematite: Improved

[127] Paracchino, A. et al. Highly active oxide photocathode for photoelectrochemical water reduction, *Nature Mater.* 10, 456-461, 2011

[128] Alexander, B. D. et al. Metal oxide photoanodes for solar hydrogen production, J. *Mater. Chem.* 18, 2298-2303, 2008

[129] Y. Liang , T. Tsubota , *J. Phys. 115* , 17594 – 17598, 2011

[130] S. K. Pilli , T. E. Furtak , L. D. Brown , T. G. Deutsch , J. a. Turner, A. M.Herring , *Energy Environ. Sci. 4,* 5028 – 5034, 2011

[131] Z. Zhao , W. Luo , Z. Li , Z. Zou , *Phys. Lett. A. 374,* 4919 – 4927, 2010

[132] D. K. Zhong , S. Choi , D. R. Gamelin , *J. Am. Chem. Soc.133* , 18370, 2011

[133] H. Ye , H. Park , A. Bard , *J. Phys. Chem. C. 115* , 12464 – 12470, 2011

[134] S. K. Pilli , T. G. Deutsch , T. E. Furtak , L. D. Brown, J. a. Turner, A. M. Herring , *Phys. Chem. Chem. Phys. 15,* 3273 – 8, 2013

[135] J. Su , L. Guo , N. Bao , C. Grimes , *Nano Lett. 11,* 1928 – 1933, 2011

[136] R. Saito , Y. Miseki , K. Sayama , *Chem. Commun. 48,* 3833 – 5, 2012

[137] S. K. Pilli , R. Janarthanan , T. G. Deutsch , T. E. Furtak , L. D. Brown , J. a. Turner , A. M. Herring , *Phys. Chem. Chem. Phys. 15,* 14723 – 8, 2013

[138] F. F. Abdi , L. Han , A. H. M. Smets , M. Zeman , B. Dam , R. van de Krol, Nat, *Commun. 4,* 2195, 2013

[139] Ki-Woong Chae et al *Beilstein J. Nanotechnol. 1,* 128–134, 2010

[140] T. C. Damien, S. P. S. Porto, and B. Tell, Phys. Rev. 142, 570, 1966

[141] C. A. Arguello, D. L. Rousseau, and S. P. S. Porto, Phys. Rev. 181, 1351, 1969

[142] J. M. Calleja and M. Cardona, Phys. Rev. B. 16, 3753, 1977

[143] D. Dohy, G. Lucazeau, and A. Revcolevschi, "Raman spectra and valence force f-ield of single-crystalline β Ga_2O_3," J. Solid State Chem. 45, 2, 180–192, 1982

[144] R. Rao, A. M. Rao, B. Xu, J. Dong, S. Sharma, and M. K. Sunkara "Blushifted Raman scattering and its correlation with the [110] growth direction in gallium oxide nanowires," J. Appl. Phys. 98, 9, 094312, 2005

[145] Miao Zhong et al, J Nanopart Res. 14, 804, 2012

[146] O. F. Schirmer and D. Zwingel, Solid State Commun. 8, 1559, 1970

[147] S. A. Studenikin, N. Golego, and M. Cocivera, J. Appl. Phys. 84, 2287 1998.

[148] X. H. Wang, D. X. Zhao, Y. C. Liu, J. Y. Zhang, Y. M. Lu, and X. W. Fan, J. Cryst. Growth. 263, 316, 2004

[149] D. M. Bagnell, Y. F. Chen, M. Y. Shen, Z. Zhu, T. Goto, and T. Yao, J. Cryst. Growth. 184-185, 605, 1998

[150] K. Vandheusen, W. L. Warren, C. H. Seager, D. R. Tallant, J. A. Voigt, and B. N. Gnade, J. Appl. Phys. 79, 7983, 1996

[151] A. F. Kohan, G. Ceder, and D. Morgan, Phys. Rev. B. 61, 15019, 2001

[152] Zhang et al j.nanoen. 120, 37, 2211-2855, 2014
[153] E. courtin J. Mater. Chem. A. 2, 6567–6577, 2014

[154] Long MC, Beranek R, Cai WM, Kisch H Hybrid semiconductor electrode for light driven photoelectrochemical switches. Electrochim Acta. 53, 4621–4626, 2008

[155] Long MC, Cai WM, Kisch H Visible light induced photoelectrochemical properties of n-$BiVO_4$ and n-$BiVO_4$/p-CO_3O_4. J. Phys Chem C 112:548–554, 2008

[156] D.Vernardou J. Mater. Chem. 21, 513–517 / 513, 2011

[157] Yi Xie et al Chem. Commun. 4542–4544, 2009

[158] M. Naeem, S. K. Hasanain and A. L. Mumtaz, "Electrical Transport and optical S- tudies of Ferromagnetic Cobalt Doped ZnO Nanoparticles Exhibiting a Metal insulator," *Journal of Physics*: *Condensed Matter*, Vol. 20, No. 2, p. 025210.doi:1088 /0953-8984/20/02/025210, 2008

[159] Ivan Grigioni J. Phys. Chem. C. 119, 20792−20800, 2015

[160] L. Irimpan, V. P. N. Nampoori, P. Radhakrishnan, B. Kri- shnan and A. Deepthy, "Size-Dependent Enhancement of Nonlinear Optical Properties in Nanocolloids of ZnO," *Journal of Applied Physics*, Vol. 103, No. 3, p. 033105. doi: 10.1063/1.283- 8178, 2008

[161] R. Al-Gaashani, S. Radiman, N. Tabet and A. R. Daud, "Ef- fect of Microwave Power on the Morphology and Optical Property of Zinc Oxide Nano-Structures Prepared via a Microwave-Assisted Aqueous Solution Method," *Materials* chemistry *and Physics*, Vol. 125, No. 3, pp. 846-852. doi:10.1016/j.matchemphys. 2010. 09.038, 2011

[162] Y. Zheng, Y. Cheng, Y. Wang, F. Bao, L. Zhou, X. Wei, Y. Zhang and Q. Zheng "A Theoretical Study of the Ion- Molecule Chemistry of K+·X Complexes (X=O, O_2, N_2, CO_2, H_2O): Implications for the Upper Atmosphere," *Journal Physical Chemistry B*, Vol. 110, No. 7, pp. 3093-3097. doi:10.1021/jp056617q, 2006

[163] Pihosh et al. small**.** *10,* No. 18, 3692–3699, 2014

[164] Gang Xin / Applied Surface Science. 256, 165–169, 2009

[165] Hong, S. J.; Lee, S.; Jang, J. S.; Lee, J. S. Heterojunction $BiVO_4$/ WO_3 Electrodes for Enhanced Photoactivity of Water Oxidation. Energy Environ. Sci. 4, 1781–1787, 2011

[166] Kay, A.; Cesar, I.; Gratzel, M. New Benchmark for water¨photoxidation by nanostructured α-Fe_2O_3 films. J. Am. Chem. Soc. 128, 15714−15721, 2006

[167] Perovskite Solar Cell Efficiency Measurements. Avoiding the Error of Making Bad Cells Look Good. J. Phys. Chem. Lett. 6, 852−857, 2015

APPENDIX A

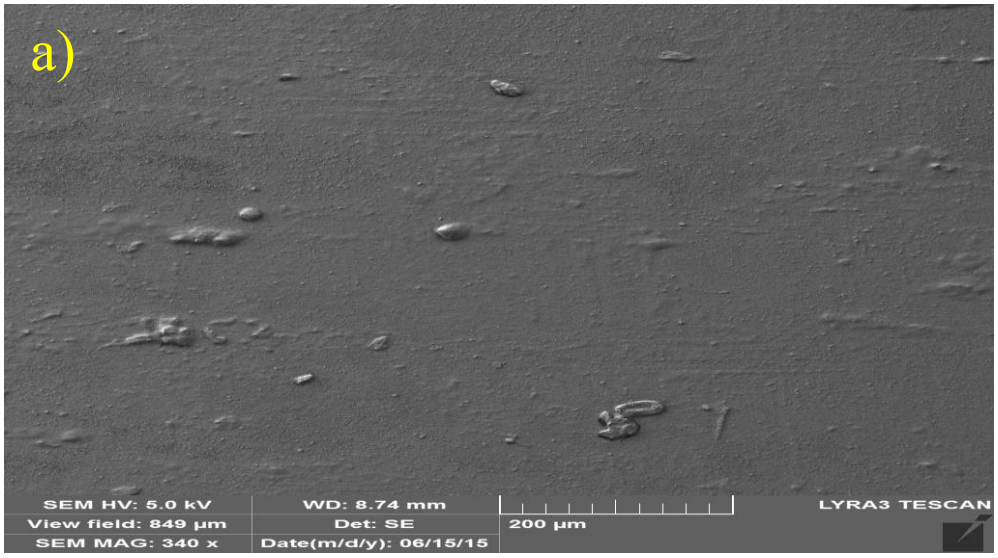

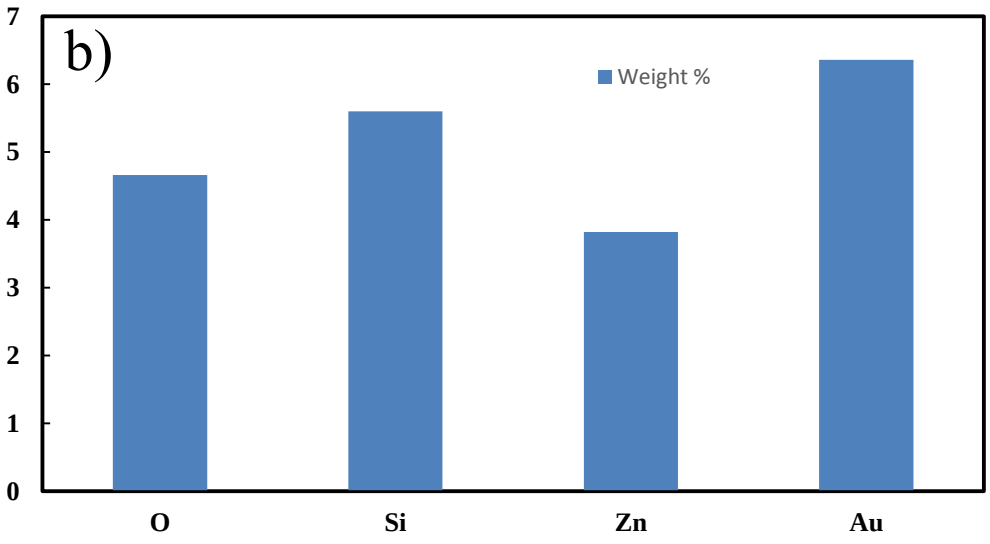

Figure 25: a) FESEM and b) EDS analysis of ZnO Seeds

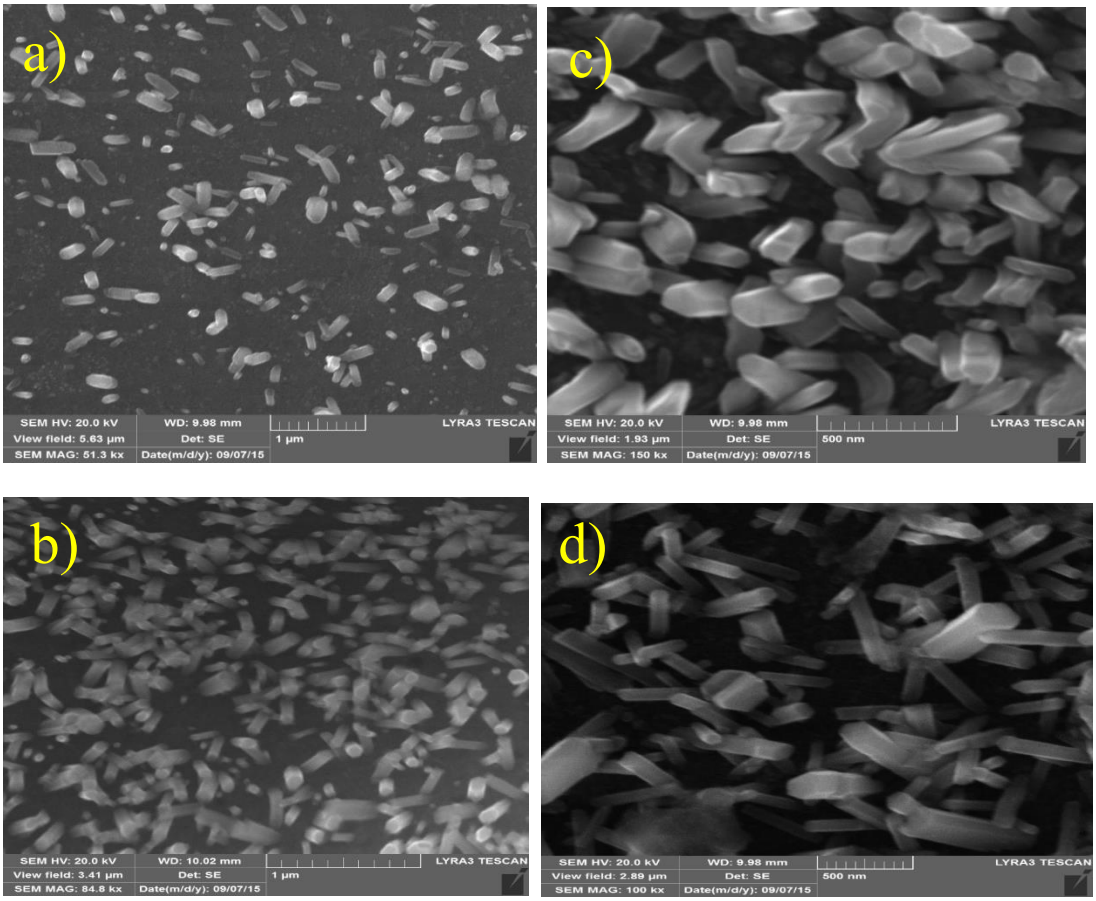

Figure 26: FESEM image at a, b) low and c, d) high magnification of 0.5 % ZnO/Ga_2O_3. 2 % and 5 % ZnO/Ga_2O_3 nanorods respectively

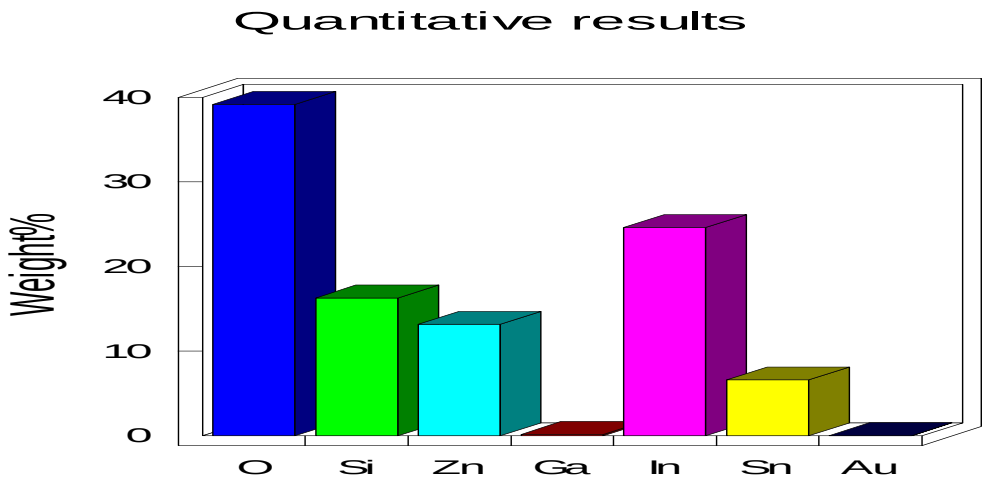

Figure 27: EDS analysis of ZnO/Ga_2O_3 nanorods

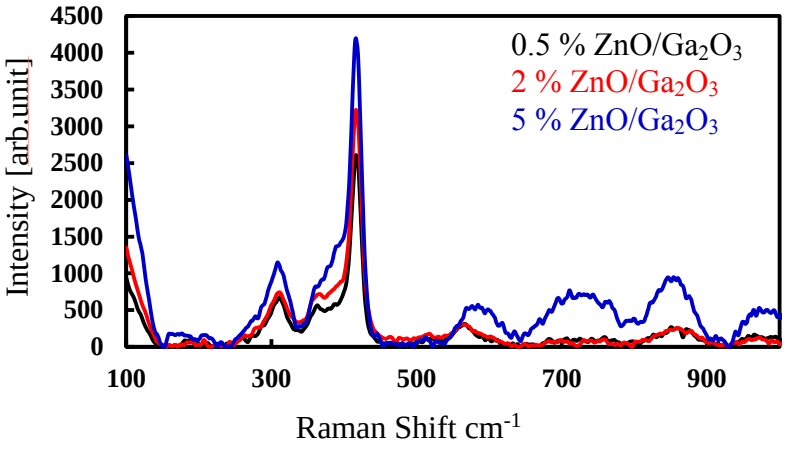

Figure 28: Raman spectrum of 0.5 %, 2 % and 5 % of ZnO/Ga_2O_3 nanorods

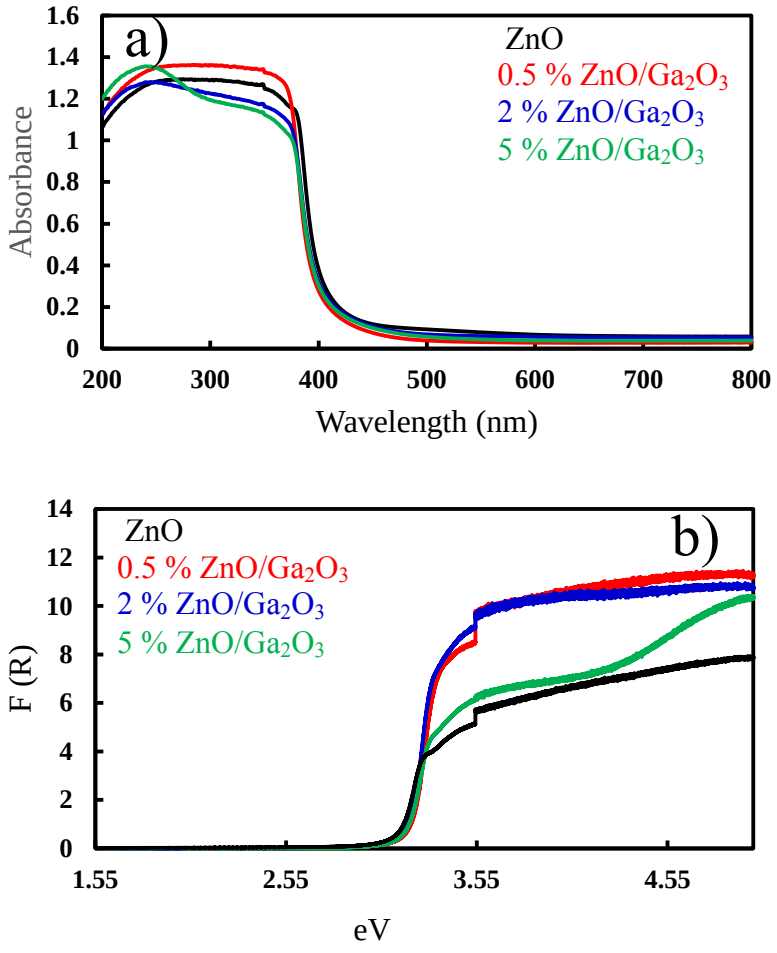

Figure 29: a) UV - VIS and b) reflectance spectrum of pure ZnO and 0.5 %, 2 %, 5 % ZnO/Ga_2O_3 nanorods

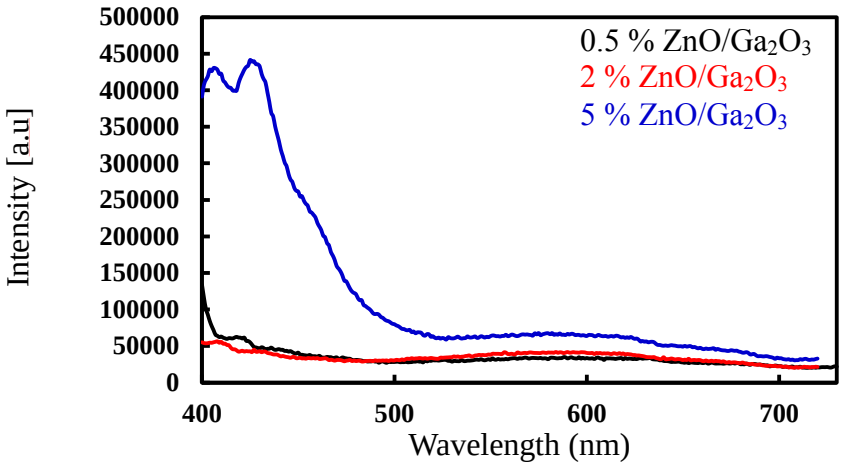

Figure 30: PL measurement of 0.5 %, 2 % and 5 % of ZnO/Ga_2O_3 nanorods

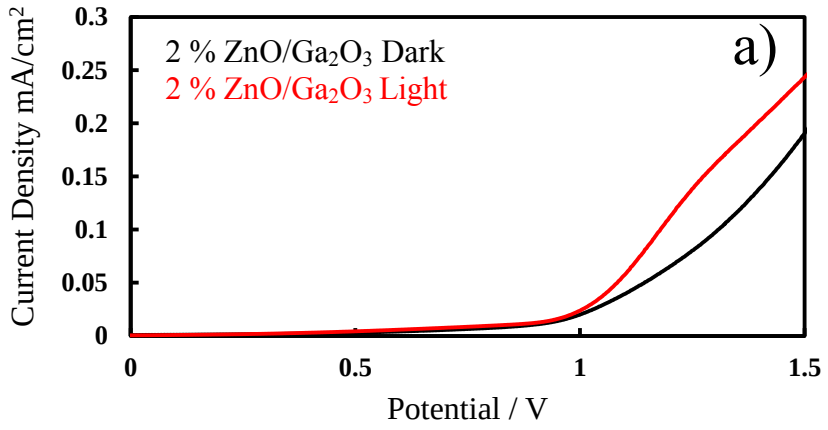

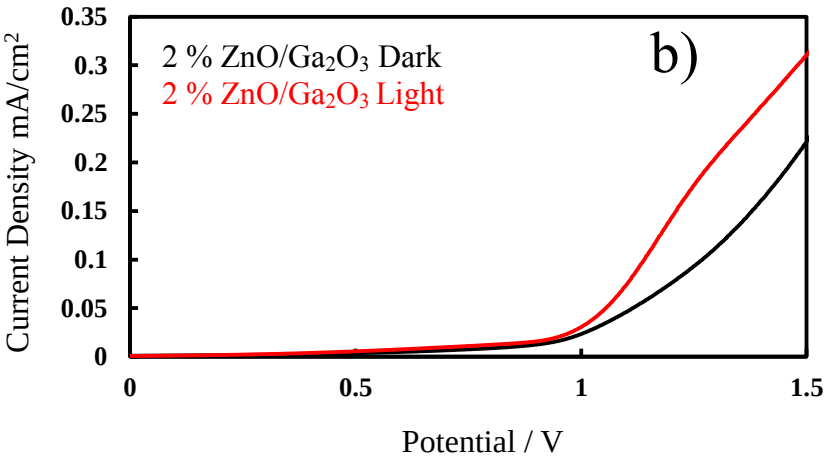

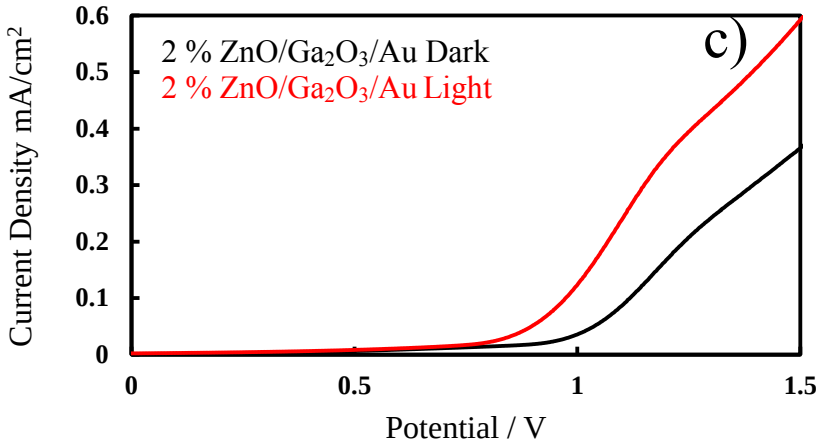

Figure 31: LSVP of a) 2 % b) 5 % ZnO/Ga_2O_3 and c) 2 % ZnO/Ga_2O_3/Au in the dark and light

APPENDIX B

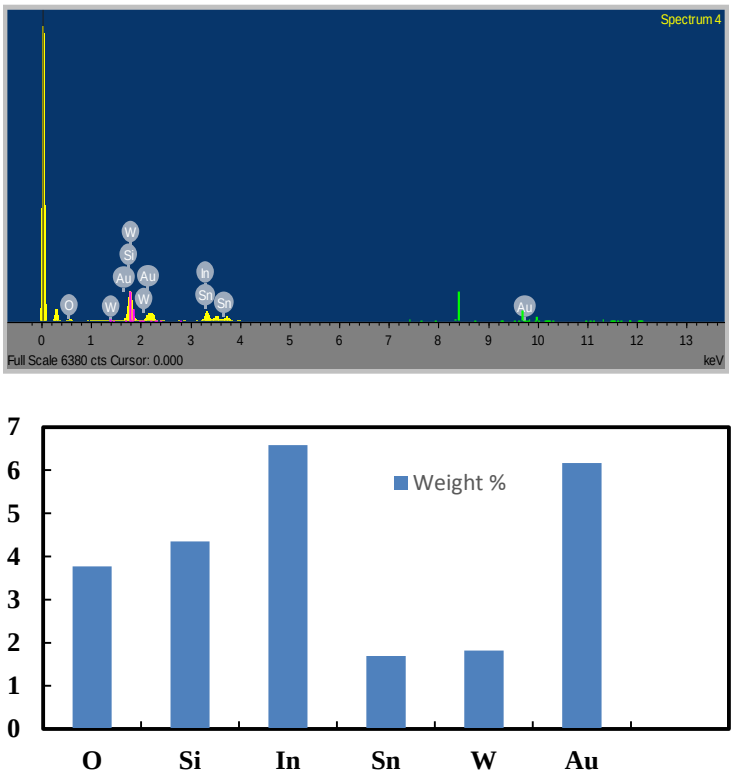

Figure 32: EDS analysis of WO_3 seeds

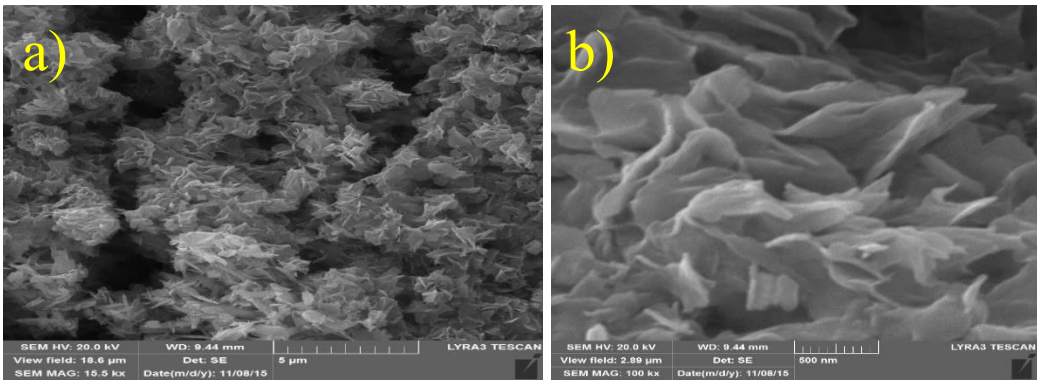

Figure 33: FESEM image of $WO_3/BiVO_4$ nanoflakes at a) low magnification b) high magnification

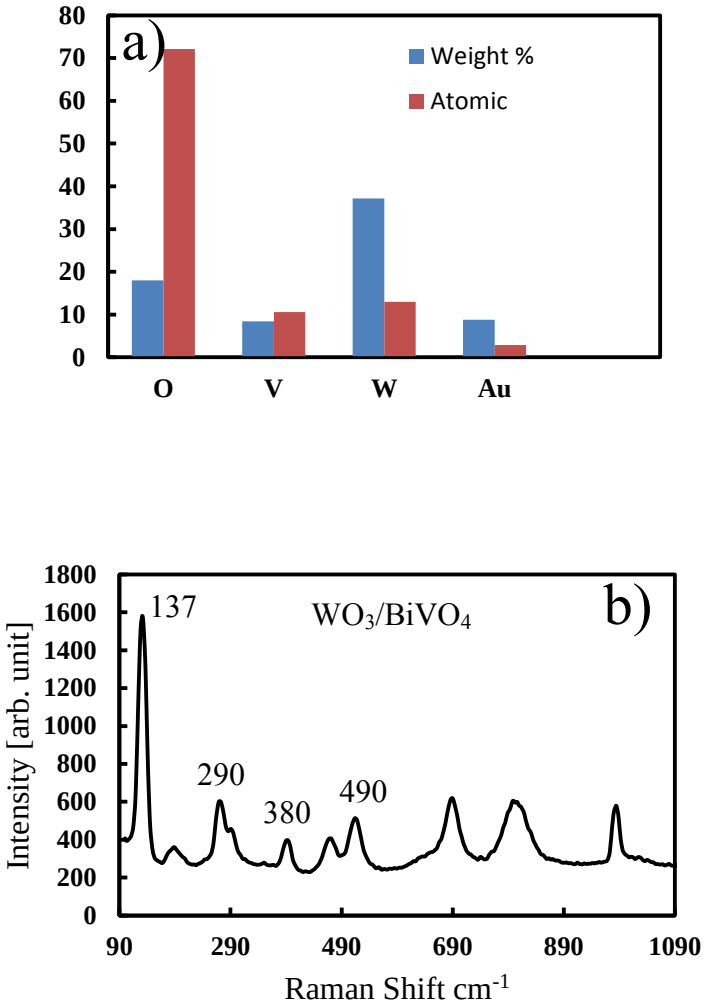

Figure 34: a) Computational analysis b) Raman spectrum of $WO_3/BiVO_4$ nanoflakes

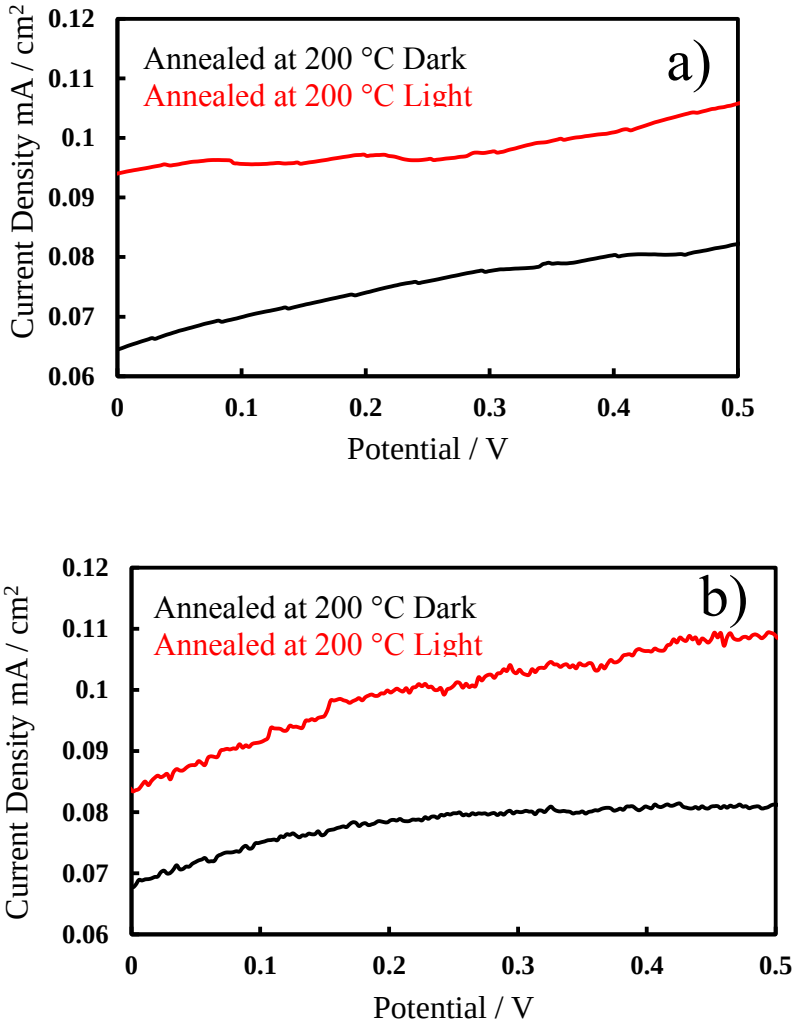

Figure 35: LSVP of $WO_3/BiVO_4$ annealed at a) 200 °C and b) 450 °C in the dark and light

VITAE

Name	: Akram Abdalla Mohammed Ibrahim
Nationality	: Sudanese
Date of Birth	: 03 / 07 / 1986
Email	: akreaaam@gmail.com
Address	: King Fahd University of Petroleum and Minerals
Academic Background	: BSc Honors degree in Chemistry from Sudan University of Science and Technology

Publications:

Akram A. M. Ibrahim, Ahsan U. Qurahi "Facile Synthesis of $WO_3/BiVO_4$ Nanoflakes as Photoanode Materials for Solar Water Splitting" (**Submitted**)

Ahsan U. Qurashi, **Akram A. M. Ibrahim,** Ibrahim Khan, Manzar Sohail "Fabrication of ZnO/ Ga_2O_3 nanorods for photoelectrochemical water splitting " (**In progress**)

-